

Astrochemistry as a tool to follow the protostellar evolution: the Class I stage

Eleonora Bianchi,^{*,†} Cecilia Ceccarelli,^{†,‡} Claudio Codella,^{‡,†} Juan Enrique-Romero,[†] Cecile Favre,[†] and Bertrand Lefloch[†]

[†]*Univ. Grenoble Alpes, CNRS, IPAG, 38000 Grenoble, France*

[‡]*INAF-Osservatorio Astrofisico di Arcetri, L.go E. Fermi 5, I-50125 Firenze, Italy*

E-mail: eleonora.bianchi@univ-grenoble-alpes.fr

Abstract

The latest developments in astrochemistry have shown how some molecular species can be used as a tool to study the early stages of the solar-type star formation process. Among them, the more relevant species are the interstellar complex organic molecules (iCOMs) and the deuterated molecules. Their analysis give us information on the present and past history of protostellar objects. Among the protostellar evolutionary stages, Class I protostars represent a perfect laboratory in which to study the initial conditions for the planet formation process. Indeed, from a physical point of view, the Class I stage is the bridge between the Class 0 phase, dominated by the accretion process, and the protoplanetary disk phase, when planets form. Despite their importance, few observations of Class I protostars exist and very little is known about their chemical content. In this paper we review the (few) existing observations of iCOMs and deuterated species in Class I protostars. In addition, we present new observations of deuterated cyanoacetylene and thioformaldehyde towards the Class I protostar SVS13-A. These new observations allow us to better understand the physical and chemical structure of SVS13-A and compare the cyanoacetylene and thioformaldehyde deuteration with other sources in different evolutionary phases.

Keywords

Astrochemistry, low-mass protostars, Class I protostars, protostellar evolution, deuteration, interstellar complex organic molecules

1. Introduction

Since the birth of radio-astronomy, a large number of simple and complex molecules have been detected in the galactic Interstellar Medium (ISM). To date around 200 molecules have been identified mainly by their rotational transition lines¹. Among them, molecular species of particular interest are the so-called interstellar complex organic molecules (hereinafter iCOMs; C-bearing molecules containing at least six atoms^{2,3}) and deuterated molecules (where one or more hydrogen atoms are substituted by deuterium ones). The former, although quite simple from a "terrestrial" chemical point of view, might represent the small bricks from which prebiotic chemistry could start. The latter have a huge diagnostic power in reconstructing the past history of the planetary system forming disk⁴. In our Galaxy, both iCOMs and deuterated species have been detected around low-mass protostars, which are nascent systems that eventually might become similar to our Solar System.

The interest in studying these two classes of molecules is, thus, twofold. On the one hand, the study of iCOMs can constrain their formation and destruction pathways in a variety of extreme physical conditions dominated by very low temperatures and densities, hugely different from those in terrestrial laboratories. This, in turn, can help to understand possible formation/destruction pathways of even more complex molecules which are impossible to detect in protostellar sources because they have a very low abundance and/or a large partition function, and which might have a role in the emergence of life. On the other hand, both deuterated and complex organic molecules are powerful diagnostic tools to study the present and the past physical conditions, namely the history of forming/formed systems⁴⁻⁷. In other words, studying the evolution of iCOMs and deuterated molecules in the different stages of star formation could help us to understand how much repro-

cessing occurs during the birth of a planetary system like our Solar System and which molecules are inherited from the early stages.

In this context, the Class I protostars represent a crucial phase: they are the bridge between the youngest protostars, dominated by the gravitational collapse, and the more evolved planetary disks, where planets and comets form. In addition, as we will discuss in detail in the next section, mounting evidence shows that planets/comets formation occurs very early, likely already in the Class I phase.

In this article, we will review what we know so far about the chemical content of Class I protostars, with a particular focus on iCOMs and deuterated molecules. We will then present new observations towards the prototype Class I source, SVS13-A, which allow us to better understand its structure and its deuterated molecular content. The structure of this article is the following: in Section 2, we describe why Class I protostars are crucial in the evolution of solar-type systems; in Section 3, we report an overview of the previous observations of iCOMs and deuterated molecules towards Class I protostars; in Section 4, we present new observations of HC_3N , DC_3N , H_2CS and HDCS towards SVS13-A and we discuss their implications in our understanding of Class I protostars; Section 5 concludes providing the future perspectives in the study of Class I protostars.

2. Class I sources, a crucial intermediate evolutionary phase in the formation of solar-type systems

2.1 Physical evolution of a solar-type protostar

The formation of a solar-type star is a complex process which lasts some Myr. It starts in dense filaments of molecular clouds and is governed by the interplay of gravitational collapse, magnetic fields and turbulence⁸⁻¹³. The current paradigm is illustrated in Figure 1, which shows the major phases of the solar-type planetary system evolution, from the prestellar cores to the formation of a planetary system¹⁴. The left panels show the spectral energy distribution (SED) of objects

representative of each phase while the right panels show actual images of objects. In the following, we briefly describe each phase.

Prestellar cores: Inside the filaments of molecular clouds, denser clumps form on scale of ~ 0.1 – 0.01 pc and some of them, called prestellar cores, slowly accrete matter towards the center under the gravitational force counteracted by the magnetic field. These objects are characterized by high central densities ($n_{H_2} > 10^4 \text{ cm}^{-3}$) and low temperatures (around 10 K or less) and are the nursery where one or more protostars are born.

Class 0 protostars: Once the collapse takes over, the material freely falls towards the center feeding the central object which, together with the infalling envelope, forms the so-called Class 0 protostar. In this stage, the central object is deeply embedded and obscured by the large infalling envelope. The Class 0 phase is dominated by the central object accretion through a rotating and accreting disk. The angular momentum is removed thanks to the ejection of gas through high-velocity and highly collimated protostellar jets.

Class I protostars: After about 10^5 yr, the protostar reaches the Class I phase in which the large-scale envelope is partially swept up. The central regions of the protostars start to be visible in the protostar SED, which is characterized by an infrared excess due to the central object light absorbed and scattered by the dusty disk and envelope.

Class II and III protostars: After about 10^6 yr, the protostar enters the Class II phase, when the envelope is almost entirely dissipated. The accretion disk becomes a protoplanetary disk, where the dust coagulation process becomes more and more efficient. The system ends up with the formation of a debris disk during the Class III phase and a final planetary system.

Thanks to observations performed at 0.96 – $3.8 \mu\text{m}$ with the SPHERE instrument, a young planet has been recently directly imaged towards the PDS 70 transition disk¹⁸. However, at present it remains difficult to directly detect planet(s) in formation (likely because of instrumental limits). While ongoing planet formation is a plausible origin of sub-structure in protoplanetary disks, it is not the only one. Many other physical processes such as large scale vortices, magnetic reconnection, and condensation fronts, have been invoked (e.g.^{19–24}). Nonetheless, hydrodynamical

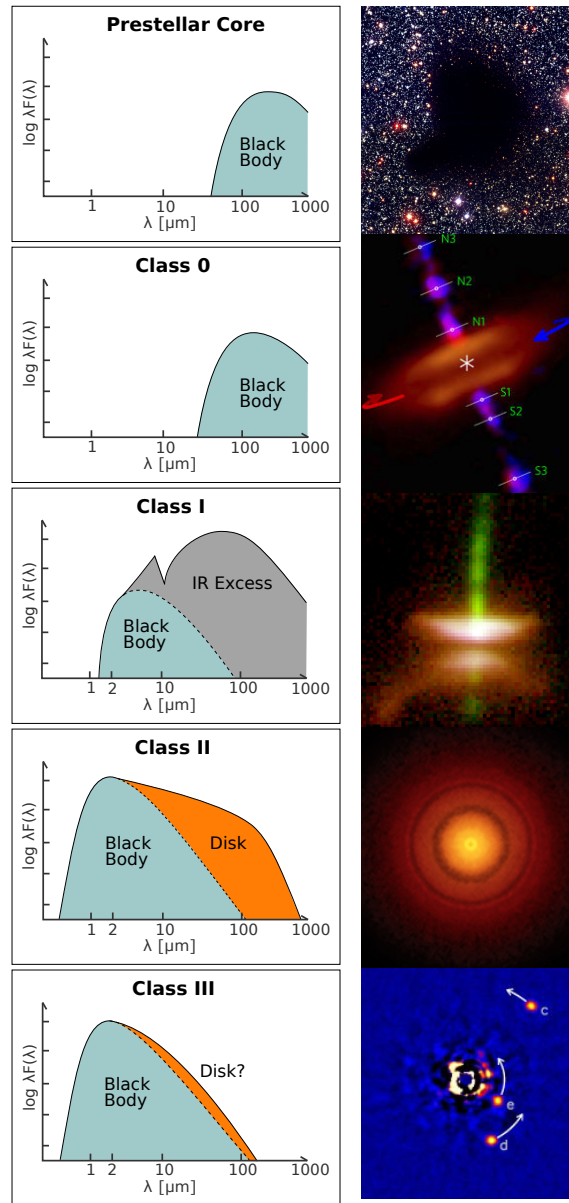


Figure 1: *Left panels:* Spectral energy distributions (SEDs) of the different formation stages of a solar-type star (adapted from¹⁵). *Right panels:* Real images of objects in the different evolutionary stages taken with different instruments. The prestellar core is the dark cloud B68 as observed by VLT/FORS1 (Credit:ESO). The Class 0 object is the HH212 protostar in Orion as observed by ALMA¹⁶. The Class I object is HH30 as observed by the Hubble Space Telescope (Credit: Chris Burrows (STScI), the WFPC2 Science Team and NASA/ESA). The Class II object is an ALMA view of the protoplanetary disc surrounding the young star TW Hydrae (Credit: S. Andrews (Harvard-Smithsonian CfA); B. Saxton (NRAO/AUI/NSF); ALMA (ESO/NAOJ/NRAO)). The Class III object is the image of the system HR 8799 with three orbiting planets. The image has been acquired at the Keck II telescope (Credit:¹⁷).

simulations predict that a planet in formation will open gaps in both dust and gas (e.g.²⁵⁻²⁷). Therefore, it remains possible to indirectly observe a forming planet through observations of the induced planet-(gas and dusty) disk interaction. In that light, ALMA observations showed that rings and gaps structure, in dust at least, seems to be a common feature in Class II protoplanetary disks of different ages (e.g.²⁸⁻³⁴). In addition, investigations of gas perturbations and/or gas kinematics motions towards the protoplanetary disks surrounding the T-Tauri star AS 209 and the Herbig object HD 163296 strongly suggest the presence of one or more embedded forming planets are present in these objects³⁵⁻³⁷.

The spectacular images provided by ALMA on protoplanetary disks suggest that planet formation could begin already at the Class I stage, earlier than previously thought. Indeed, the recent observations of the HL Tau system³⁸ showed several sharp rings and gaps in the disk which could indicate the presence of nascent planets³⁹. The youth of this system, thought to be ≤ 1 Myr old, in a transition stage between Class I and II, indicates that planet formation could start during the early Class I stage. Several studies have been dedicated to the measurement of the disk masses in Class I sources^{40,41} with the intent to determine the initial mass budget for forming planets. Recent studies in fact indicate that the protostellar disk mass is already set near the onset of the Class 0 protostellar stage and remains roughly constant during the Class I protostellar stage⁴².

In summary, the Class I protostars promise to be the best targets to study the initial conditions of planet formation, especially from the chemical point of view, since their envelope+disk system is still massive enough to be detected and, hence, studied with millimeter telescopes and interferometers.

2.2 Evolution of the iCOMs content

The different evolutionary phases described above correspond to different degrees of complexity of matter chemical composition (see e.g.^{4,5,43}). In the following, we briefly describe the evolution of iCOMs in the different phases.

Prestellar cores: At the low temperatures found in molecular clouds and prestellar cores, atoms and molecules in the gas phase freeze-out onto the cold surfaces of the dust grains. Hydrogenation of these frozen atoms and molecules takes place on the grain surfaces, forming icy mantles, mostly composed of water (H_2O). Relevant to this article, the frozen CO is hydrogenated and forms formaldehyde (H_2CO) and methanol (CH_3OH)^{44,45}. These simple hydrogenated species are detected in the solid-phase via infrared observations⁴⁶. More complex species, notably some iCOMs such as methyl formate (HCOOCH_3) and dimethyl formate (CH_3OCH_3), are detected in the gas phase towards prestellar cores^{47–52}. It is not clear yet how these iCOMs are synthesised. In principle, at these low temperatures, no grain surface reactions other than hydrogenation can occur nor can these large molecules be released from the grain surfaces into the gas-phase. Thus, it is proposed that they form via gas-phase reactions from simple species like methanol, injected from the grain mantles by non-thermal desorption processes^{53,54}.

Class 0 protostars: During the Class 0 phase, the forming central object increasing luminosity warms up the surrounding envelope. Where the temperature reaches about 100 K, the grain mantles sublimate, giving origin to the so-called hot corinos^{3,5}. In these objects, a plethora of iCOMs (more than a dozen³) are detected in relatively large abundances, similar to the methanol one^{55–58}. The synthesis of iCOMs in hot corinos is debated. One possibility is that, during the warming up of the envelope, atoms and radicals, previously formed and frozen in the mantles, acquire mobility and react on the grain surfaces forming iCOMs^{59,60}. Then, at about 100 K the entire mantle sublimates injecting into the gas-phase the iCOMs formed in this way. Theoretical chemistry studies, however, show that this combination of radicals does not necessarily end up in iCOMs^{61,62}. Alternatively, the mantle simple molecules (such as methanol or formaldehyde) formed during the prestellar phase are injected into the gas at 100 K and undergo reactions that form iCOMs^{63–65}.

Class I protostars: Section 3.1 will review the status of the art, but we anticipate that, unfortunately, very little is known about the iCOMs census and abundance in Class I protostars.

Protoplanetary disks: In protoplanetary disks, very few iCOMs have been detected so far: methanol (CH_3OH), methyl cyanide (CH_3CN) and formic acid (HCOOH)^{66–68}. The obvious ques-

tion is: are more complex molecules not detected in protoplanetary disks only because of the current instrument detection limits or chemistry changes from the Class 0 to the protoplanetary disk phase? The fact that the existing detections are all at the 5σ level definitely points to instrumental limits, and further study of iCOMs content in Class I protostars might answer this question.

In summary, Class I sources are, from an evolutionary point of view, the connection between the Class 0 protostars and the protoplanetary disks (see previous Section). However, it remains unclear whether this is also true from a chemical point of view. Analogously, the degree of reprocessing of the chemical content from the earlier to the late evolutionary stages is still poorly constrained. Some similarities observed in the molecular abundances of Solar System comets (e.g. 67P/Churyumov-Gerasimenko) and young protostars^{7,69,70} seem to suggest that something could survive the journey. The interest for Class I protostars is even higher when we think that the nascent planetary atmospheres could be linked to the early disk chemical composition.

2.3 Molecular deuteration as an evolutionary indicator

The process of deuteration consists of an enrichment of the amount of deuterium with respect to hydrogen in molecular species. Despite the very low level of the D/H elementary abundance ($\sim 1.6 \cdot 10^{-5}$)⁷¹, molecules in cold ISM show a high ratio, up to 13 orders of magnitude larger than the elemental one⁷².

Deuterated molecules have been observed in all the stages of the solar-type star formation process, from prestellar cores^{73–78}, to Class 0^{72,79–83} and protoplanetary disks^{84–89}. These observations are a powerful tracer of the evolution during the formation of a solar-type planetary system⁴. Fig. 2 shows the deuteration measured for water and organic molecules at different stages of the solar-type star formation process, from prestellar cores to Solar System objects. The figure suggests a general decreasing trend which can be interpreted as a modification of the gas chemical content. In particular, the deuteration of organics, considering different molecular tracers, decreases up to two orders of magnitude going from Class 0 protostars to the Solar System objects such as comets and carbonaceous chondrites⁴. However, measurements of deuteration in protoplanetary

disks are based on the detection of DCN and DCO⁺ in few objects^{47,66,84,85,87-93}. Moreover, in these objects the emission is probably tracing the disk surface, due to substantial disk midplane freeze-out. Given the difficulty so far to observe other large deuterated molecules in disks that trace more closely to the midplane, it would be very useful to understand if changes in deuteration occur already during the protostellar stages.

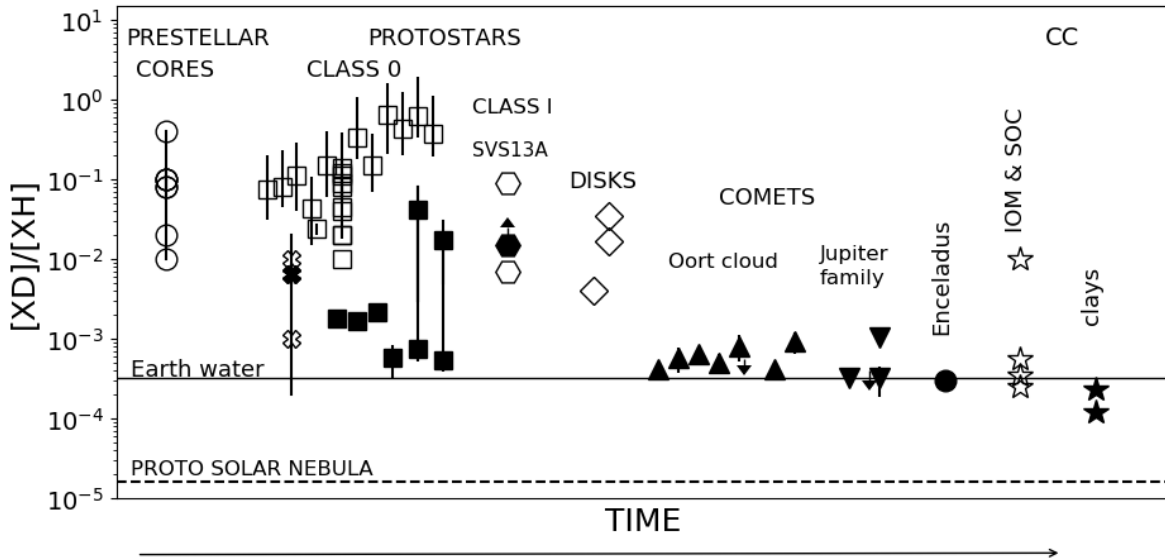


Figure 2: Molecular deuteration ratio of ISM and Solar System objects (adapted from⁴). The filled symbols refer to water whereas open symbols refer to organic matter. Note that for organic matter, different molecular tracers are used. The measurements of prestellar cores deuteration, indicated with circles are from^{77,78,94}. Class 0 protostars are indicated with squares and are from^{81,95-98}. The previous data have been updated with the last measurements at a Solar System scale provided by the ALMA PILS survey^{82,99,100} and HH212¹⁰¹. The crosses indicate deuteration measurements in the protostellar shock region L1157-B1^{102,103}. The Class I measurements (hexagons) refer to SVS13-A, specifically to the following molecular species: formaldehyde⁶, methanol⁶ and water¹⁰⁴. The diamond symbols refer to deuteration measurements in protoplanetary disks⁸⁴⁻⁸⁶.

Briefly, the molecular deuteration is enhanced in cold environments and it is mostly, but not exclusively, caused by the enhancement of the H₂D⁺ abundance with respect to the H₃⁺ one. This is the molecule that, in molecular gas, transfers the deuterium from HD to the other molecules (see⁴ for more details). The major parameters that influence the molecular deuteration are gas temperature¹⁰⁵, CO abundance in the gas phase^{73,106} and H₂ ortho-to-para ratio^{107,108}.

As mentioned above, in protostellar objects the measured degree of deuteration can be up to 13 orders of magnitude larger than the elementary value and it is different for each molecular species⁵. In general, the external region of the protostellar envelopes (at larger radii than 100 au) shows gas conditions very similar to that observed in prestellar cores. The measured molecular deuteration in these regions is therefore very likely representative of the current gas conditions. On the contrary, the molecular content in hot corinos is dominated by the ice mantle sublimation (see above). Therefore, molecular deuteration measured in these regions is dominated by deuteration at the time of mantle formation and, consequently, can give us information on past chemical gas conditions and the history of the mantle formation^{4,5,79,102,109}. Water, for example, that is mostly formed in molecular clouds, presents a lower degree of deuteration with respect to formaldehyde and methanol, which are very likely formed during the prestellar phase. Interestingly, based on the deuteration measurement, recent modeling studies suggest that interstellar water ice is largely inherited by forming disks without significant alteration^{110–112}.

3. iCOMs and molecular deuteration in Class I protostars

In this Section, we review what is known, namely observed, about iCOMs and molecular deuteration in Class I protostars.

3.1 iCOMs

Several observations have been carried out so far with single-dish telescopes in the mm-spectral range to detect iCOMs in samples of Class 0 and Class I protostars (see e.g.^{113–120}). However, no clear results have been obtained so far regarding the chemical content modification during the evolutionary transition from Class 0 to Class I, because of the lack of surveys dedicated to Class I protostars. This is also related to the instrumental limitation of single-dish telescopes, which provide a relatively small angular resolution and large beam dilution, severely affecting the observations of compact and weak sources such as Class I protostars. For example, some Class I

protostars have been included in a survey performed using the IRAM-30m with angular resolution larger than $20''$ ^{117,118,120–122}. As a result, iCOMs are almost non-detected or detected via very low excitation lines. Moreover, these surveys often derive low rotational temperatures, which suggests that the detected iCOMs lines might not originate in the hot corinos.

SVS13-A has been so far the only Class I source for which a complete census of the iCOMs (with abundances larger than about 10^{-9}) has been possible⁷. The source will be described in detail in the next Section; here we anticipate that it has a hot corino surrounded by a cold envelope, namely a structure similar to a Class 0 protostars, but with a less massive envelope.

The iCOMs census towards SVS13-A was obtained in the framework of the IRAM-30m Large Program ASAI (Astrochemical Surveys At IRAM: Lefloch et al.¹²⁰), which obtained unbiased spectral surveys of several solar-type protostars, entirely covering the 1, 2 and 3 mm wavelength bands observable from ground. Given the small size of the SVS13-A hot corino ($\lesssim 1''$), iCOMs were mostly detected in the 1mm band, less affected by the beam dilution. The large spectral range covered by the survey allowed us to detect more than 100 lines from different iCOMs and, consequently, to accurately determine the lines excitation conditions and the iCOMs column densities. In particular, we derived rotational temperatures between 35 and 110 K, and column densities between 3×10^{15} and 1×10^{17} cm² on the $0.3''$ size previously determined by interferometric observations of glycolaldehyde¹²³. Figure 3 shows some of the measured abundance ratios towards SVS13-A. The abundance ratio of some key iCOMs such as acetaldehyde, dimethyl ether and ethanol with respect to methyl formate are compared for Class 0 sources and SVS13-A and two other Class I sources, whose values are from the literature^{118,119,121}. These species are of particular interest because they are abundant and they can give us information on different formation mechanisms. For comparison, the figure also reports the abundance ratios measured in comets⁶⁹ and in the molecular-rich protostellar shock L1157-B1^{124,125}. The iCOMs abundances are normalized to methyl formate to avoid opacity problems which could affect other more abundant species such as methanol. Strictly speaking, this figure suggests that when iCOMs are detected in Class I sources, the iCOM composition appears similar to what is seen at the Class 0 stage. More loosely,

the chemical richness of Class I protostars is comparable to that of Class 0 sources. Therefore, the chemical complexity could be inherited from the previous stages, although the comparison is practically based on only one Class I source, SVS13-A, which may not be representative of the whole Class I. For the other two Class I sources, the measurements are mostly only upper limits. A larger sample of source is needed to confirm this picture.

Recently, two Class I sources from the Serpens cluster were observed using ALMA interferometer¹²⁶. Only one of them, the source Ser-emb 17, shows iCOMs emission from CH₃OH, CH₃OCH₃, HCOOCH₃, NH₂CHO and CH₂CO. The abundance ratios of iCOMs with respect to methanol in this source are comparable to that measured in the other two Class 0 Serpens sources contained in the sample, Ser-emb 1 and Ser-emb 2, confirming that suggested by the analysis of SVS13-A.

3.2 Molecular deuteration

As mentioned in Section 2.3, deuterated molecules have been detected in all the stages of Sun-like star formation, from the prestellar core stage to the Solar System objects⁴ but no clear results have been obtained so far for the intermediate Class I evolutionary phase. The first indications a possible decrease of the deuteration with the evolutionary stage came from measurements of the double deuterated formaldehyde in star-forming regions¹³³. Other measurements of deuteration in Class I sources¹³⁴ included only few transitions and sampled large regions (up to 58''), well beyond the protostellar system. In addition, a low deuteration of formaldehyde was reported towards R CrA IRS7B, a low-mass protostar in the Class 0/I transitional stage¹³⁵. However, in this case the envelope chemical composition is probably altered by the external UV irradiation from the nearby Herbig Ae star R CrA so that the low deuteration ratio cannot be interpreted as an evolutionary trend.

In SVS13-A, the singly deuterated formaldehyde (HDCO) is ~ 0.09 with respect to formaldehyde⁶, a value similar to the average one measured in Class 0 protostars (~ 0.12 ⁸¹), as shown in Fig. 4. Please note that this comparison only refers to Class 0 protostars observed with the same single-

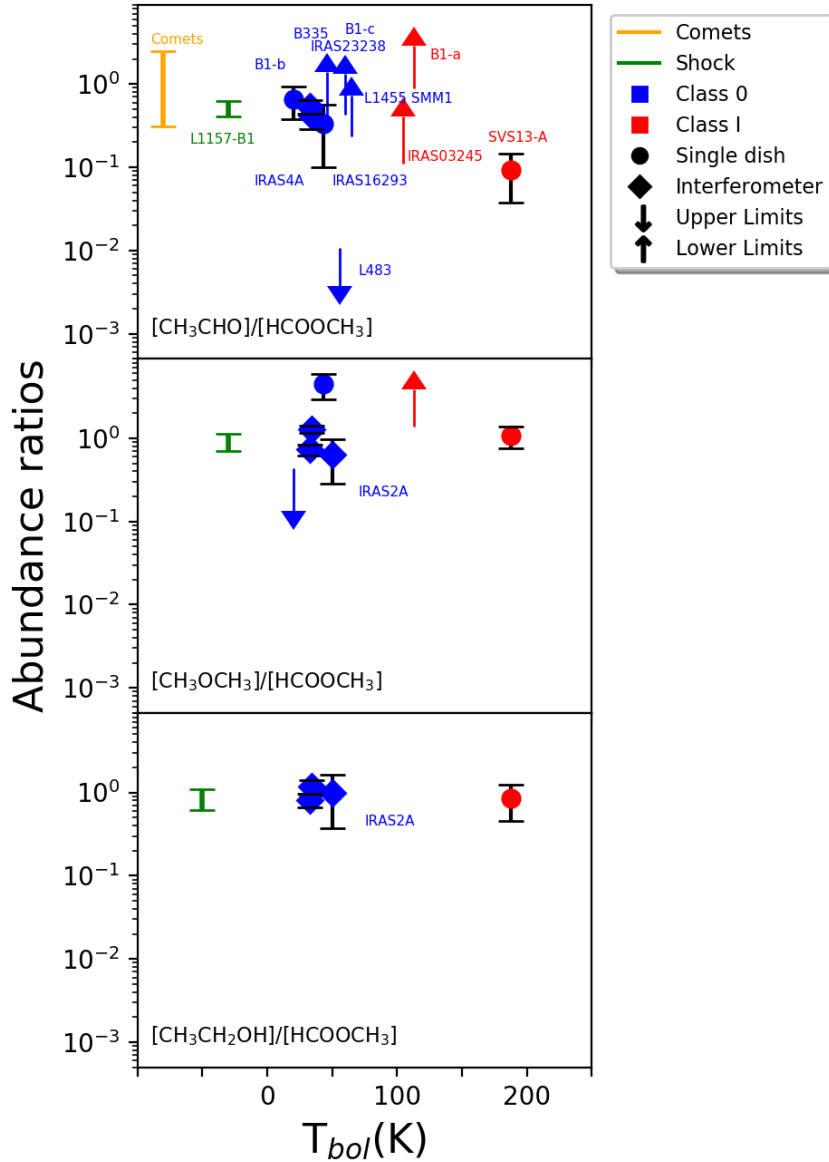


Figure 3: Figure adapted from⁷. Abundance ratios of the iCOMs detected in SVS13-A compared to different sources, as indicated in the upper panel. The sources are: the pre-protostar hydrostatic core B1-b^{127,128}; the Class 0 sources IRAS4A, IRAS2A^{56,129}, IRAS16293–2422 (e.g.^{57,100,130}), B1-c^{118,121}, IRAS23238+7401^{119,121}, L1455 SMM1^{119,121}, IRAS19347+0727 in B335¹³¹ and L483¹³²; the protostellar shock L1157-B1^{124,125}, the Class I sources B1-a^{118,121}, IRAS03245+3002^{119,121} and SVS13-A⁷; comets⁶⁹. Blue symbols indicate Class 0 protostars while red symbols are for Class I protostars. Circles indicate single-dish measurements while diamonds are for interferometric measurements. Arrows indicate upper limit measurements. The abundance ratios of comets and the protostellar shock L1157-B1 are reported for comparison using an orange line and a green line, respectively. Note that in these cases the x-value has no meaning.

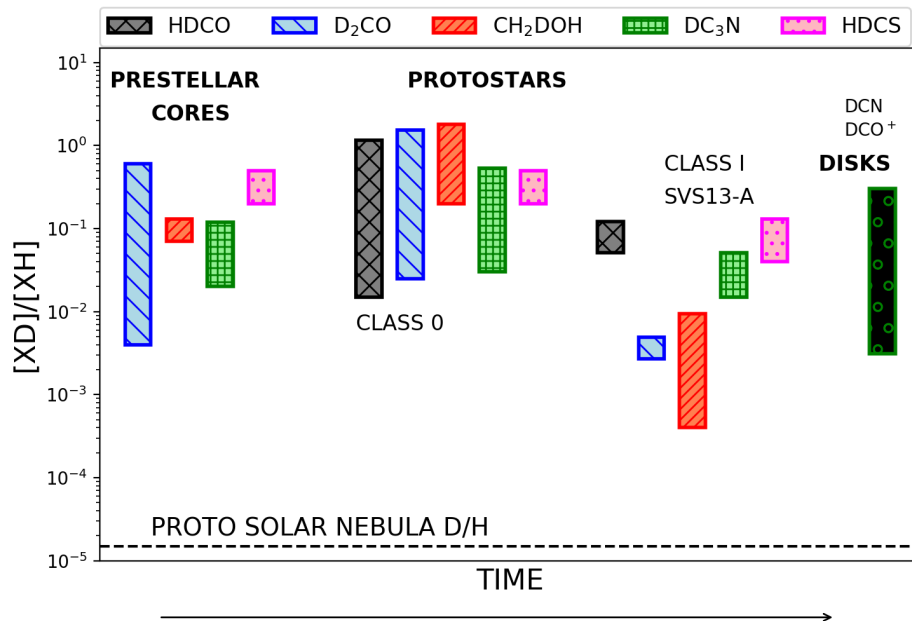


Figure 4: $[XD]/[XH]$ ratio measured in organic matter in different astronomical sources: prestellar cores (D_2CO ⁷³, CH_2DOH ⁷⁷, DC_3N ¹³⁶⁻¹³⁸, and $HDCS$ ^{139,140}), Class 0 protostars ($HDCO$ ⁸¹, D_2CO ⁸¹, CH_2DOH ⁸¹, DC_3N ¹⁴¹, and $HDCS$ ⁷⁰). SVS13-A data refer to the deuteration of $HDCO$ (8.6×10^{-2}), D_2CO (3.8×10^{-3})⁶, CH_2DOH (7.1×10^{-3} for the hot corino and 1.5×10^{-3} for a larger region, i.e. a radius ≤ 350 au)⁶, DC_3N ($1.5 - 3.6 \times 10^{-2}$, this work), and $HDCS$ ($4 - 9 \times 10^{-2}$, this work). Protoplanetary disks data refer to measurements of DCN/HCN and DCO^+/HCO^+ ^{47,84,85,87-90,92}. Figure adapted from⁶. We have to note that opacity can strongly affect the main isotopologues abundances and then the $[XD]/[XH]$ derivation (see text).

dish telescope (IRAM-30m): measurements obtained with higher resolution (e.g. with ALMA) show lower levels of deuteration, which may be due to the different probed spatial scales, namely the fact that multiple physical components are present in the line of sight. Therefore, we emphasize that comparisons based on single-dish data have to be taken with caution.

With this caution in mind, the deuteration measured using doubly deuterated formaldehyde (D_2CO) and singly deuterated methanol (CH_2DOH) is one and two orders of magnitude lower, respectively, than that measured towards Class 0 protostars^{6,81} (see Figure 4). We have to caution, though, that methanol deuteration in Class 0 sources suffers from uncertainty in the opacity of the lines used to derive CH_3OH column density⁸¹. For example, the new analysis of the Class 0 source IRAS4A, obtained with ASAI and that includes $^{13}CH_3OH$ lines, shows that the CH_3OH column density is underestimated by about a factor of ten if not corrected for the opacity (Lefloch, private communication). When considering all these uncertainties, it is not totally clear whether the molecular deuteration is preserved from Class 0 to Class I. In summary, accurate opacity estimations together with more observations of both Class 0 and Class I sources are needed to draw firm conclusions.

4. New tracers of molecular deuteration towards the Class I protostar SVS13-A

In this section, we present new observations of HC_3N and H_2CS and their deuterated counterparts towards the Class I protostar SVS13-A. Before reporting the new observations and their analysis, we briefly describe SVS13-A, which is the prototype Class I protostar where most of the chemical studies have been carried out so far.

4.1 Source background

SVS13-A is a Class I protostar belonging to the SVS13 cluster, which is composed of at least five objects. It is part of the NGC 1333 molecular cloud in Perseus, and its distance has been accurately

measured by GAIA to be 299 ± 14 pc¹⁴².

Since the discovery of the first dark clouds by Barnard in 1913, the Perseus region has received increasing attention and has been extensively investigated at many wavelengths and with a variety of spatial resolutions. In particular, the young cluster NGC 1333 is one of the best studied and the most active region of star formation in the Perseus cloud complex. The region is rich in sub-mm cores, embedded Young Stellar Objects (YSOs), radio continuum sources, masers, IRAS sources, SiO molecular jets, H₂ and Herbig-Haro shocks, molecular outflows, and the lobes of extinct outflows^{143–147}. Far Infrared and sub-millimeter observations of the southern region revealed many bright Class 0/I protostars, including the famous ones, SVS13, IRAS2 and IRAS4. Successive high spatial resolution observations showed that many of them are actually binary and even multiple systems. Further molecular line observations of the region highlighted the importance of protostellar outflows in the matter distribution of NGC 1333. As an example, Lefloch et al.¹⁴⁴ showed the presence of two large cavities excavated by the outflows ejected from newly formed stars.

SVS13-A itself is associated with an extended outflow (> 0.07 pc^{144,146}) as well as with the famous chain of Herbig-Haro (HH) objects 7–11¹⁴³. IRAM-30m observations revealed that the SVS13 star forming region is associated with a YSOs cluster dominated in the millimeter by two objects, called A and B, which are separated by $\sim 15''$ ^{148,149}. A third source, SVS13-C, is located farther away at a distance of $20''$ from A¹⁴⁹. At smaller scales (≤ 100 au), the region is even more complex than previously thought, as SVS13-A is itself a binary system, separated by $0'.3$ (30 au)^{150,151} (see Figure 5; Bianchi et al. in preparation).

Interestingly, SVS13-A and SVS13-B seem to be in two different evolutionary phases. SVS13-B is a bona fide Class 0 protostar of $L_{\text{bol}} \simeq 1.0 L_{\text{sun}}$ ^{147,152} which drives a well collimated SiO jet^{145,153}. SVS13-A definitely has a larger luminosity, ($L_{\text{bol}} \simeq 32.5 L_{\text{sun}}$ ¹⁴⁷), a low $L_{\text{submm}}/L_{\text{bol}}$ ratio ($\sim 0.8\%$) and a high bolometric temperature ($T_{\text{bol}} \sim 188$ K,¹⁴⁷). Thus, although still deeply embedded in a large scale envelope¹⁴⁴, SVS13-A is considered a Class I protostar.

A systematic study of the molecular lines towards SVS13-A has revealed the presence of a hot

corino region via the detection of warm (≥ 150 K) and very compact (~ 25 au in diameter) HDO emission¹⁰⁴. Later, De Simone et al.¹²³ imaged the line emission from a iCOM, glycolaldehyde, around SVS13-A confirming the existence of a hot corino with size of $0''.3$, corresponding to ~ 90 au in diameter. More studies then aimed to better characterize the properties of the SVS13-A hot corino. Bianchi et al.⁶ showed that methanol is very abundant in the hot corino and measured its gas temperature to be around 100 K (as expected). The SVS13-A hot corino is rich in iCOMs, showing emission from the classical ones, namely acetaldehyde, methyl formate, dimethyl ether, ethanol, and formamide⁷. Finally, a formaldehyde multiple-line analysis showed the presence of a cold (~ 20 K) and relatively extended (~ 1500 au in diameter) envelope surrounding the SVS13-A hot corino⁶.

When it comes to the measurement of the molecular deuteration in SVS13-A, only that of methanol and formaldehyde has been measured before the present work. The $\text{CH}_2\text{DOH}/\text{CH}_3\text{OH}$ abundance ratio in the hot corino is 0.007 ± 0.002 whereas in the extended envelope the $\text{HD}\text{CO}/\text{H}_2\text{CO}$ and $\text{D}_2\text{CO}/\text{H}_2\text{CO}$ abundance ratios are 0.09 ± 0.04 and 0.004 ± 0.001 , respectively⁶.

4.2 Observations and results

We report new observations obtained within the IRAM-30m Large Project ASAI¹²⁰. The data were acquired during several runs between 2012 and 2014 using the broad band EMIR receiver, connected to FTS200 backends, with a spectral resolution of 200 kHz. The rms noise (in T_{MB} scale) is about 2 mK, 7 mK, 9 mK in a channel of 0.6 km s^{-1} , 0.4 km s^{-1} , and 0.2 km s^{-1} for the 3, 2, and 1 mm spectral windows, respectively. The observations pointed towards SVS13-A, namely at $\alpha_{\text{J2000}} = 03^{\text{h}} 29^{\text{m}} 03^{\text{s}}.76$, $\delta_{\text{J2000}} = +31^{\circ} 16' 03''.0$, and they were acquired in wobbler switching mode (with a $180''$ throw). The pointing was found to be accurate to within $3''$. The telescope HPBWs lies from $\simeq 9''$ at 276 GHz to $\simeq 30''$ at 80 GHz.

Data reduction and lines Gaussian fit have been performed using the GILDAS-CLASS¹ package. Besides the errors on the Gaussian fit, the calibration uncertainties are estimated to be $\simeq 20\%$.

¹www.iram.fr/IRAMFR/GILDAS/

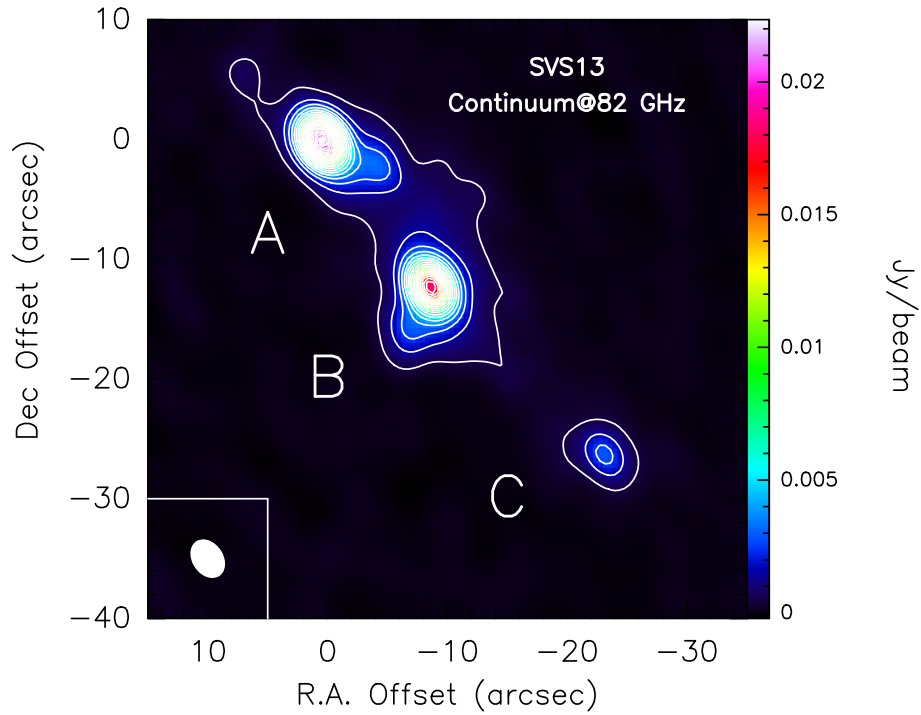


Figure 5: Continuum observations at 82 GHz of the SVS13 system performed using the IRAM-NOEMA interferometer. The observations are performed in the framework of the Large Program SOLIS (Seeds Of Life In Space³). The beam size is $3.5'' \times 2.6''$ while the position angle (PA) is 31° . The SVS13 system is composed by 3 main sources. SVS13-A, in the upper left, is the brighter source in the millimeter and it is classified as a Class I protostar (see text). It has been recently resolved into a close binary system, separated by $0''.3$. SVS13-B is a younger Class 0 source, located $\sim 15''$ south-east with respect to SVS13-A. Finally, in the lower right of the map there is a third source, SVS13-C which is located at a distance of $20''$ from A.

For a more detailed description of the ASAI observations we refer the reader to¹²⁰.

4.2.1 Cyanoacetylene

We detected 13 and 7 lines from cyanoacetylene and its deuterated form DC₃N, respectively. The excitation energies, E_{up} , cover the range 20–165 K and 22–69 for HC₃N and DC₃N respectively.

Examples of the detected line spectra are shown in Figure 6. Table 1 reports the detected transitions and the observational parameters. The peak velocities of the detected HC₃N and DC₃N lines are between +7.7 and +9.0 km s⁻¹, being consistent, once the fit and the calibration uncertainties are considered, with the systemic source velocity. The line profiles are close to a Gaussian shape. The line FWHMs are between 1.1 and 2.8 km s⁻¹ for the main isotopologue and between 0.4 and 1.9 km s⁻¹ for the deuterated isotopologue.

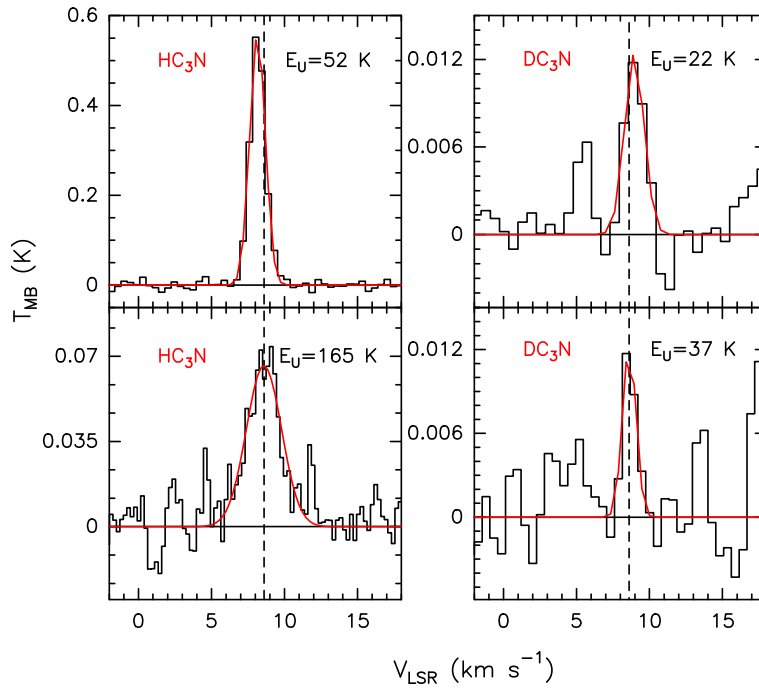


Figure 6: Examples of the observed spectra of HC₃N and DC₃N, in T_{MB} scale (i.e. not corrected for the beam dilution): species and excitation energies are reported in the upper left and right corner of each panel, respectively. The vertical dashed line stands for the ambient LSR velocity (+8.6 km s⁻¹)¹⁵².

Table 1: List of transitions and line properties (in T_{MB} scale) of the DC₃N and HC₃N emission detected towards SVS13-A.

Transition	ν^a (GHz)	HPBW ($''$)	E_{up}^a (K)	$S\mu^{2a}$ (D ²)	rms (mK)	T_{peak}^b (mK)	V_{peak}^b (km s ⁻¹)	$FWHM^b$ (km s ⁻¹)	I_{int}^b (mK km s ⁻¹)
DC ₃ N									
DC ₃ N 10–9, F=9–8	84.4298	29	22	124					
DC ₃ N 10–9, F=10–9	84.4298	29	22	137	6	31 (1)	+8.72 (0.13)	1.0 (0.3)	34 (8)
DC ₃ N 10–9, F=11–10	84.4298	29	22	152					
DC ₃ N 11–10, F=10–9	92.8724	26	27	138					
DC ₃ N 11–10, F=11–10	92.8724	26	27	151	2	12 (1)	+8.96 (0.10)	1.6 (0.2)	21 (3)
DC ₃ N 11–10, F=12–11	92.8724	26	27	166					
DC ₃ N 12–11, F=11–10	101.3148	24	31	152					
DC ₃ N 12–11, F=12–11	101.3148	24	31	165	1	12 (1)	+8.82 (0.02)	1.9 (0.1)	24 (1)
DC ₃ N 12–11, F=13–12	101.3148	24	31	180					
DC ₃ N 13–12, F=12–11	109.7571	22	37	166					
DC ₃ N 13–12, F=13–12	109.7571	22	37	179	1	12 (1)	+8.62 (0.05)	1.1 (0.1)	14 (1)
DC ₃ N 13–12, F=14–13	109.7571	22	37	194					
DC ₃ N 16–15, F=15–14	135.0832	18	55	208					
DC ₃ N 16–15, F=16–15	135.0832	18	55	221	1	39 (1)	+8.40 (0.01)	0.5 (0.1)	19 (1)
DC ₃ N 16–15, F=17–16	135.0832	18	55	235					
DC ₃ N 17–16, F=16–15	143.5249	17	62	222					
DC ₃ N 17–16, F=17–16	143.5249	17	62	235	3	18 (3)	+7.76 (0.06)	0.7 (0.1)	14 (2)
DC ₃ N 17–16, F=18–17	143.5249	17	62	249					
DC ₃ N 18–17, F=17–16	151.9664	16	69	235					
DC ₃ N 18–17, F=18–17	151.9664	16	69	249	12	20 (4)	+8.94 (0.20)	0.4 (0.7)	8 (6)
DC ₃ N 18–17, F=19–18	151.9664	16	69	263					
HC ₃ N									
HC ₃ N 9–8	81.8815	30	20	125	9	642 (41)	+9.00 (0.01)	1.4 (0.02)	947 (13)
HC ₃ N 10–9	90.9790	27	24	139	3	613 (35)	+8.60 (0.01)	1.5 (0.008)	950 (4)
HC ₃ N 10–11	100.0764	25	29	153	3	587 (30)	+8.43 (0.01)	1.4 (0.008)	880 (5)
HC ₃ N 12–11	109.1736	23	34	166	4	526 (17)	+8.46 (0.01)	1.3 (0.01)	747 (5)
HC ₃ N 15–14	136.4644	18	52	208	9	562 (12)	+8.16 (0.01)	1.2 (0.02)	745 (11)
HC ₃ N 16–15	145.5609	17	59	222	14	540 (18)	+8.34 (0.01)	1.1 (0.03)	654 (14)
HC ₃ N 17–16	154.6573	16	67	236	9	426 (18)	+8.16 (0.01)	1.2 (0.02)	521 (9)
HC ₃ N 18–17	163.7534	15	75	250	8	380 (22)	+8.37 (0.01)	1.3 (0.03)	524 (9)
HC ₃ N 23–22	209.2302	12	120	319	11	175 (10)	+8.47 (0.03)	1.9 (0.08)	353 (13)
HC ₃ N 24–23	218.3248	11	131	333	12	166 (12)	+8.64 (0.03)	2.1 (0.1)	375 (14)
HC ₃ N 25–24	227.4189	11	142	347	10	125 (7)	+8.50 (0.04)	2.2 (0.1)	292 (12)
HC ₃ N 26–25	236.5128	10	153	361	10	87 (9)	+8.41 (0.05)	2.1 (0.1)	196 (11)
HC ₃ N 27–26	245.6063	10	165	374	11	66 (8)	+8.60 (0.09)	2.8 (0.3)	199 (15)

^a Frequencies and spectroscopic parameters of DC₃N and HC₃N have been extracted from the Jet Propulsion Laboratory data base¹⁵⁴. ^b The errors in brackets are the Gaussian fit uncertainties.

4.2.2 Thioformaldehyde

The ASAI spectra detected 11 lines of thioformaldehyde and 5 lines of its single deuterated isotopologue HDCS. The line excitation energies E_{up} are in the range 35–165 K and 31–64 K for H_2CS and HDCS, respectively. Examples of the detected line spectra are shown in Figure 7; the detected transitions and the observational parameters are listed in Table 2. The line profiles are close to a Gaussian shape and the peak velocities are close to the systemic source velocity, with values between +7.6 and +8.7 km s^{-1} for H_2CS and between +7.8 and +8.4 km s^{-1} for HDCS. The line FWHM range is 1.8–3.8 km s^{-1} for the main isotopologue and 0.7–2.3 km s^{-1} for the single deuterated isotopologue. All the transitions of H_2CS and HDCS are detected in the ASAI 1mm band, except for one transition of HDCS detected at 2mm.

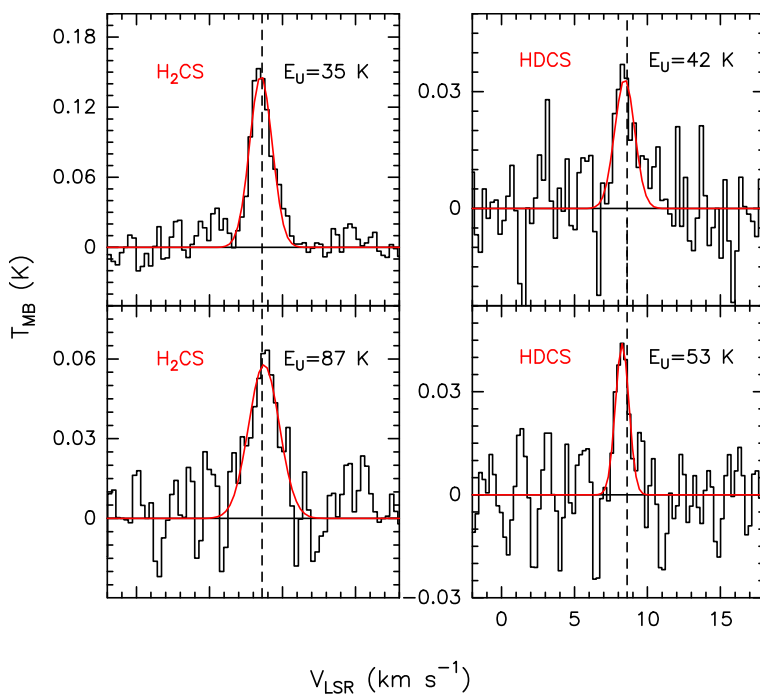


Figure 7: Examples of the observed spectra of H_2CS and HDCS, in T_{MB} scale (i.e. not corrected for the beam dilution): species and excitation energies are reported in the upper left and right corner of each panel, respectively. The vertical dashed line stands for the ambient LSR velocity (+ 8.6 km s^{-1} ; ¹⁵²).

Table 2: List of transitions and line properties (in T_{MB} scale) of the HDCS and H₂CS emission detected towards SVS13-A.

Transition	ν^a (GHz)	$HPBW$ ($''$)	E_{up}^a (K)	$S\mu^{2a}$ (D ²)	rms (mK)	T_{peak}^b (mK)	V_{peak}^b (km s ⁻¹)	$FWHM^b$ (km s ⁻¹)	I_{int}^b (mK km s ⁻¹)
HDCS									
HDCS 5 _{1,5} -4 _{1,4}	151.9275	16	31	13	7	31 (7)	+8.36 (0.11)	1.1 (0.3)	37 (7)
HDCS 7 _{1,7} -6 _{1,6}	212.6483	12	50	19	9	39 (4)	+7.81 (0.08)	0.7 (0.2)	29 (6)
HDCS 7 _{0,7} -6 _{0,6}	216.6624	12	42	19	10	33 (5)	+8.44 (0.18)	1.6 (0.4)	57 (12)
HDCS 8 _{0,8} -7 _{0,7}	247.4885	10	53	22	9	22 (3)	+8.27 (0.09)	1.1 (0.2)	51 (9)
HDCS 8 _{1,7} -7 _{1,6}	252.7350	10	64	21	3	27 (2)	+8.32 (0.05)	2.3 (0.2)	67 (3)
H ₂ CS									
o-H ₂ CS 6 _{1,6} -5 _{1,5}	202.9241	12	47	47	24	222 (27)	+8.45 (0.06)	2.0 (0.2)	468 (33)
p-H ₂ CS 6 _{0,6} -5 _{0,5}	205.9879	12	35	16	27	147 (12)	+8.53 (0.10)	1.8 (0.3)	283 (31)
p-H ₂ CS 6 _{2,4} -5 _{2,3}	206.1586	12	87	15	11	58 (10)	+8.74 (0.11)	2.5 (0.3)	153 (13)
o-H ₂ CS 6 _{1,5} -5 _{1,4}	209.2006	12	48	48	13	181 (12)	+8.37 (0.03)	1.8 (0.1)	351 (15)
o-H ₂ CS 7 _{1,7} -6 _{1,6}	236.7270	10	59	56	13	175 (13)	+7.82 (0.04)	2.4 (0.1)	448 (16)
p-H ₂ CS 7 _{0,7} -6 _{0,6}	240.2669	10	46	19	12	110 (9)	+8.56 (0.06)	2.8 (0.2)	333 (16)
p-H ₂ CS 7 _{2,6} -6 _{2,5}	240.3821	10	99	17	30	74 (16)	+8.05 (0.27)	3.3 (0.6)	262 (41)
o-H ₂ CS 7 _{3,5} -6 _{3,4}	240.3930	10	165	47	27	90 (13)	+7.65(0.21)	3.8 (0.5)	362 (40)
o-H ₂ CS 7 _{3,4} -6 _{3,3}	240.3938	10							
p-H ₂ CS 7 _{2,5} -6 _{2,4}	240.5491	10	99	17	9	45 (11)	+8.16 (0.13)	3.2 (0.3)	153 (13)
o-H ₂ CS 7 _{1,6} -6 _{1,5}	244.0485	10	60	56	10	178 (12)	+8.49 (0.03)	2.9 (0.1)	556 (13)
o-H ₂ CS 8 _{1,8} -7 _{1,7}	270.5219	9	72	64	15	124 (11)	+8.46 (0.07)	2.9 (0.2)	384 (18)

^aFrequencies and spectroscopic parameters of HDCS and H₂CS have been extracted from the Cologne Database for Molecular Spectroscopy¹⁵⁵. ^bThe errors in brackets are the gaussian fit uncertainties.

4.3 Non-LTE analysis of the line emission

We analysed the HC₃N and H₂CS observed lines via the non-LTE large velocity gradient (LVG) approach using the model described by Ceccarelli et al.¹⁵⁶. For HC₃N, we used the collisional coefficients with H₂ from Faure et al.¹⁵⁷, provided by the BASECOL database¹⁵⁸. For H₂CS, we used the collisional coefficients with H₂ computed for the H₂CO–H₂ system by Wiesenfeld & Faure¹⁵⁹, scaled for the different mass, and provided by the LAMDA database¹⁶⁰. In the calculations, we assumed a Boltzmann distribution for the H₂ ortho-to-para ratio.

We ran two large grids of models varying the gas temperature, T_{kin} , from 20 to 200 K; the H₂ density, n_{H_2} , from 1×10^5 to $2 \times 10^8 \text{ cm}^{-3}$; the HC₃N column density, $N(\text{HC}_3\text{N})$, from 1×10^{12} to $4 \times 10^{16} \text{ cm}^{-2}$; the H₂CS column density, $N(\text{H}_2\text{CS})$, from 1×10^{13} to $4 \times 10^{16} \text{ cm}^{-2}$. We then found the solution with the lowest χ^2 , in the temperature-density-column density-size space.

4.3.1 Cyanoacetylene

The Spectral Line Energy Distribution (SLED) of the detected lines is shown in Fig. 8. It is obvious looking at the SLED that the emitting gas is composed of (at least) two components. So, we searched for a fit with two components. We obtained a good fit (see Fig. 8) with the parameters reported in Table 3 and that indicates the presence of a cold (~ 20 K) extended component, likely associated with the extended envelope and/or molecular cloud, and a second lukewarm (~ 40 K), more compact and denser one, whose origin will be discussed later.

Table 3: Results from the non-LTE LVG analysis. Columns reports the derived gas temperatures, T_{kin} , density n_{H_2} , column densities, N_{tot} , and size, θ for the two components traced by the HC₃N line emission.

T_{kin} (K)	n_{H_2} (cm^{-3})	N_{tot} (cm^{-2})	θ ($''$)
20 K – 30 K	1×10^5	2×10^{12}	45
40 K	8×10^6	1×10^{13}	9

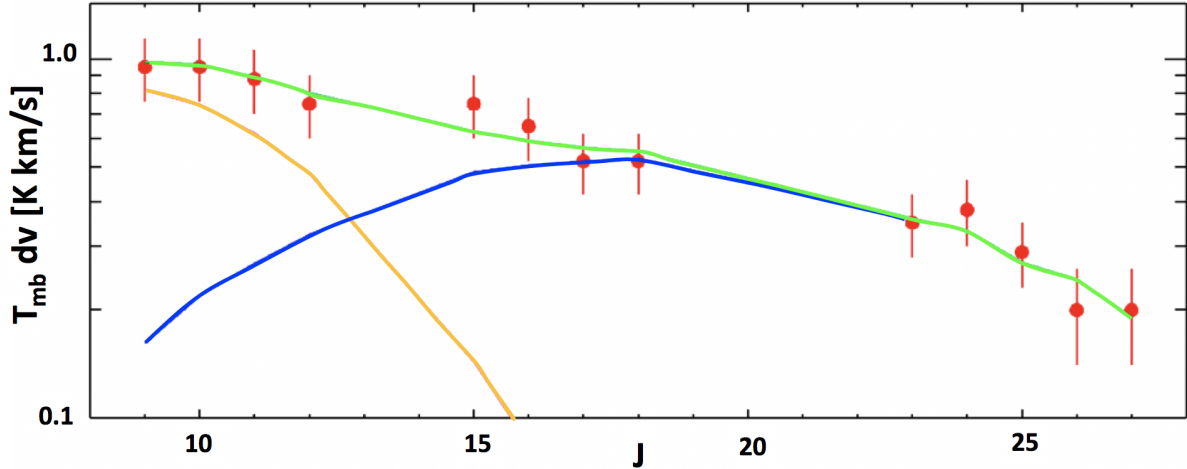


Figure 8: Observed (red points) and theoretical (curves) line intensity of the H_3CN lines as a function of the quantum number J . The best fit (green curve) of the lines is obtained considering two different components: one extended region ($45''$) with $N(\text{H}_3\text{CN})=2 \times 10^{12} \text{ cm}^{-2}$, $T_{\text{kin}}=20\text{K}-30 \text{ K}$ and a density of $1 \times 10^5 \text{ cm}^{-3}$ (orange curve) and a second component with a size of $9''$, $N(\text{H}_3\text{CN})=1 \times 10^{13} \text{ cm}^{-2}$, $T_{\text{kin}}=40 \text{ K}$ and a density of $8 \times 10^6 \text{ cm}^{-3}$ (blue curve).

4.3.2 Thioformaldehyde

In the case of H_2CS , one component fits very well with all the measured line intensities, as shown in Fig. 9. The H_2CS column density and emitting size are well constrained: $N(\text{H}_2\text{CS})=6 \times 10^{15} \text{ cm}^{-2}$ and $\theta=0'.6$ (equivalent to $\sim 120 \text{ au}$). On the contrary, the density and temperature are degenerate and not well constrained: both a $40-60 \text{ K}$ and $n_{\text{H}_2} \geq 8 \times 10^4 \text{ cm}^{-3}$ or a $60-100 \text{ K}$ and $n_{\text{H}_2} \leq 3 \times 10^5 \text{ cm}^{-3}$ component give the same χ^2 . The origin of this component will be discussed in Section 5. Finally, we notice that, in order to have a good fit, the H_2CS ortho-to-para ratio has to be equal to 3, namely the statistical value.

4.3.3 Deuterated cyanoacetylene and thioformaldehyde

We derived the deuteration of cyanoacetylene and thioformaldehyde by dividing the intensities of lines with the same J number for $\text{DC}_3\text{N}/\text{HC}_3\text{N}$ and similar upper level energy, E_{up} , for $\text{HDCS}/\text{H}_2\text{CS}^{161}$. This method has a twofold advantage with respect to the commonly used one that consists in dividing column densities derived by rotational diagrams: it allows us to determine the deuteration with

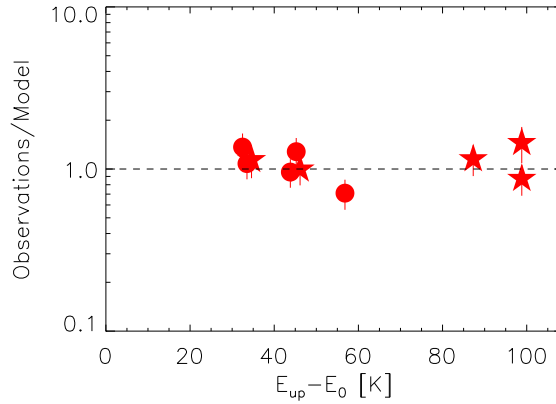


Figure 9: Ratio between the observed and the best-fit theoretical line intensities of H_2CS as a function of the line upper level energy (see text). Stars and circles indicate para- and ortho- transitions, respectively.

a (much) lower error and as a function of the energy of the transition, which can then provide precious information on the deuteration in the different components of the emitting gas. Please note that we corrected the intensities of the main isotopologues to account for the optical depths estimated from the LVG analysis, described in two previous sections. Similarly, we took into account the H_2CS ortho-to-para ratio derived in the previous section.

Figure 10 shows the deuteration of the two molecules, cyanoacetylene and thioformaldehyde, as a function of the upper level energy of the transition E_{up} , namely their excitation conditions: roughly, the larger E_{up} the warmer and/or denser the emitting gas. The molecular deuteration varies from $\sim 3.5\%$ to $\sim 1.5\%$ in HC_3N with increasing E_{up} , while it goes from $\sim 4\%$ to $\sim 9\%$ in H_2CS . Therefore, it seems that while the molecular deuteration decreases in warmer/denser HC_3N emitting gas, it increases in the H_2CS emitting gas. We will discuss the possible meaning of this different behavior in Section 5.

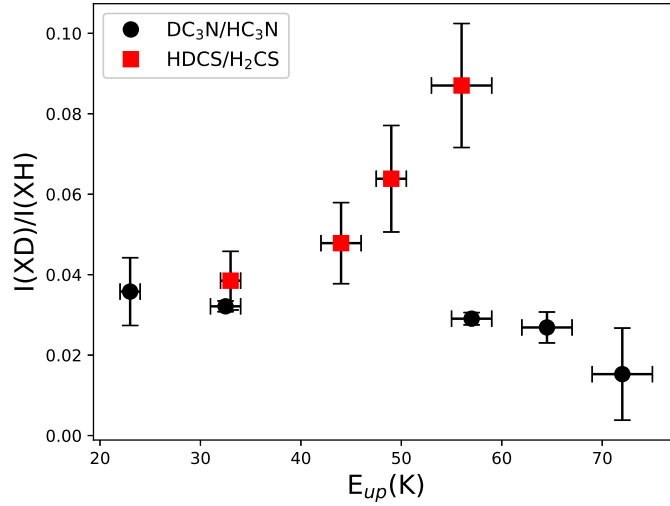


Figure 10: Deuteration ratio of HC₃N (black points) and H₂CS (red squares) as a function of the line upper level energy E_{up} . Please note that the E_{up} of the line is linked to its excitation conditions so that larger E_{up} likely trace warmer and/or denser gas.

5. Discussion

5.1 Deuterated cyanoacetylene and thioformaldehyde across SVS13-A

In the previous section, we have shown a puzzling, at first sight, behavior of the deuteration of cyanoacetylene and thioformaldehyde: while the former decreases with increasing upper level energy of the lines E_{up} , namely the excitation conditions of the lines, the latter decreases with increasing E_{up} . This is, at first sight, rather puzzling. However, we will show here that this is completely explicable when one considers the physical and chemical structure of SVS13-A. Therefore, we will start from that.

5.1.1 Physical and chemical structure of SVS13-A

The analysis of our new observations reported in Section 4.3 helps to understand the physical and chemical structure of SVS13-A, its hot corino and surrounding envelope. The hot corino, namely the region with temperatures greater than about 100 K, has a radius of about 45 au and is enriched with HDO, CH₃OH and other iCOMs. The density of the hot corino is not well constrained, only

a lower limit of $\sim 10^8 \text{ cm}^{-3}$ is obtained. On the other hand, the HC_3N line emission identifies an extended region, with a radius of about $\sim 7000 \text{ au}$, with a temperature of about 20 K and density of about 10^5 cm^{-3} . In between these two regions, there is the lukewarm envelope with intermediate temperatures, $\sim 40 \text{ K}$, and densities, $\sim 10^6 - 10^7 \text{ cm}^{-3}$, traced by H_2CO and HC_3N . Very likely, the innermost part of the lukewarm envelope is the region where H_2CS emits the lines that we observe.

The intriguing behavior of the HC_3N and H_2CS deuteration as a function of increasing line excitation conditions, shown in Fig. 10, can now be interpreted in the light of the structure described in Section 5.1 and provides information on the history of SVS13-A.

5.1.2 $\text{DC}_3\text{N}/\text{HC}_3\text{N}$

Cyanoacetylene is located in the cold and lukewarm envelope and it is, extremely likely, formed by gas-phase reactions occurring in the present (mostly from the reaction of C_2 with CN)^{162,163}. Therefore, it is totally natural that lines with increasing E_{up} , which probe gas with increasing temperatures, show a decreasing molecular deuteration as they reflect the deuteration caused by the present gas-phase $\text{H}_2\text{D}^+/\text{H}_3^+$ abundance ratio, which decreases with increasing temperature⁴. We emphasize the relatively large value of the measured $\text{DC}_3\text{N}/\text{HC}_3\text{N}$ ratio (0.01–0.04), which points to a substantial depletion of gaseous CO in the envelope of SVS13-A^{73,106}. Indeed, gas-phase CO destroys the H_2D^+ ion that is responsible for the formation in the gas-phase of most deuterated species.

5.1.3 $\text{HDCS}/\text{H}_2\text{CS}$

Thioformaldehyde is present in the innermost regions of the lukewarm envelope, at about 40–60 K. It is very likely produced on the grain-surfaces by the hydrogenation of frozen CS, even though no laboratory experiments nor theoretical calculations exist in the literature to substantiate this hypothesis. The CS ($\sim 0.77 \text{ ea}_a$) dipole moment is larger than that of CO ($\sim 0.39 \text{ ea}_0$), although

the electronegativity of atomic S is closer to that of C than O². This probably implies that CS gets adsorbed on the icy surfaces of dust grains much easier than CO, and, hence, that H₂CS is formed relatively fast. H₂CS would then be injected into the gas-phase when the dust temperature reaches the iced-H₂CS sublimation temperature. Unfortunately, no laboratory measurements of the binding energy of H₂CS on icy surfaces are available. The only theoretical estimate, based on the interaction of one molecule of H₂CS with two water molecules rather than the whole ice structure, gives a value of ~ 3000 K¹⁶⁵. This would correspond to a sublimation of frozen H₂CS when the dust temperature reaches about 40—60 K, which is surprisingly consistent with the region where we detect H₂CS in SVS13-A.

We can now try to interpret why HDCS/H₂CS increases in warmer/denser regions, as shown by Fig. 10. In general, the molecular deuteration of hydrogenated species on the grain-surfaces increases with decreasing gaseous CO abundance at the time of ice formation, namely with increasing density¹⁰⁹. We showed above that the envelope of SVS13-A is centrally peaked, namely the density increases going inward. There is no reason to think that this was not the case at the time of the iced H₂CS formation. Therefore, going inwards corresponds to ices that are more and more deuterated, which is what we see in the HDCS/H₂CS abundance ratio.

5.2 Comparison with other sources

Figure 2 summarises the deuteration found in different molecules and different sources. In this section, we will focus on the cyanoacetylene and thioformaldehyde deuteration, the other species having been discussed in Section 3.2.

5.2.1 DC₃N/HC₃N

The value of cyanoacetylene deuteration measured in SVS13-A (0.01–0.04) is similar to that found from previous measurements towards cold cores (0.02–0.1)^{136,137}. It is also similar to that found to-

²Interestingly, though, the CS dipole moment enhancement comes from the contribution of both the charges on each atom and the induced dipoles on either C and S atoms which add up instead of partially cancelling, as it is the case for CO¹⁶⁴.

wards the first hydrostatic core Chamaeleon-MMS1 (~ 0.04)¹³⁸ and in the Class 0 protostar L1527 (~ 0.03)¹⁴¹.

More recently, cyanoacetylene deuteration has been measured towards the Class 0 protostar IRAS16293-2422¹⁶³, where it was found that DC_3N/HC_3N varies from 0.5 in the cold envelope to 0.05 in the hot corino region. As in the case of SVS13-A, the deuteration in the cold envelope is likely a present-day gas-phase product. The larger measured DC_3N/HC_3N value indicates a more substantial depletion of gaseous CO in IRAS16293-2422 than in SVS13-A (see above), which is in agreement with SVS13-A being more evolved (namely with a globally warmer envelope) than IRAS16293-2422. The absence of HC_3N in the hot corino of SVS13-A, contrarily to IRAS16293-2422, maybe due to a slower formation of the prestellar core from which SVS13-A originates, following the arguments presented by Jaber et al.¹⁶³.

5.2.2 HDCS/H₂CS

The thioformaldehyde deuteration measured in SVS13-A (0.04–0.10) is not very different, within the errors, to that measured in IRAS 16293-2422 ($HDCS/H_2CS=0.1\pm 0.014$)⁷⁰, the only Class 0 protostar where HDCS/H₂CS has been also measured. The deuteration of H₂CS has been previously measured in the dark cloud Barnard 1 (~ 0.3)¹³⁹, and in the prestellar core L1544¹⁴⁰. The measured value is 0.20 ± 0.14 , again similar, within the error bars, to that measured towards SVS13-A.

5.2.3 Conclusive remarks

Looking at Fig. 2, there does not seem to exist a dramatic decrease of cyanoacetylene and thioformaldehyde going from the prestellar core to the Class I protostar phases. However, from the discussion above it is clear that the information is too scarce to be able to assess whether the lack of a trend can be linked to a lack of evolution in the deuteration of cyanoacetylene and thioformaldehyde with time. In addition, it is also clear that the specific conditions of each object where the deuteration is measured enter into the equation and could even be the dominant effect, as is the

case when comparing, for example, the $\text{DC}_3\text{N}/\text{HC}_3\text{N}$ in the Class 0 protostar IRAS16293-2422 and the Class I protostar SVS13-A.

6. Conclusions and perspectives

In this contribution, we argued that Class I protostars are the bridge between the youngest Class 0 protostar phase and the more evolved Class II/III, where it is believed planets and comets form in their protoplanetary disks. Analogously, we argued that Class I protostars are crucial objects to study the chemical evolution throughout the solar-type star forming process and to understand what is passed from one stage to the successive one.

We then presented a review of the chemical properties of Class I, specifically focused on the iCOMs and deuterated molecules and showed that most of the information about Class I protostars comes from studies towards SVS13-A. The first obvious conclusion, therefore, is that the information is extremely scarce and that many more observations are necessary to carry out a meaningful comparison among different evolutionary stages.

Having said that, our preliminary conclusions are:

- The complete census of iCOMs emission performed in SVS13-A suggests that the chemical richness of Class I protostars is comparable to that of Class 0 sources.
- The comparison of the deuteration of methanol seems rather to indicate a decrease in Class I sources. However, we cautioned on the large uncertainties linked to the limited observations available.
- The new observations presented here allow us to reconstruct the physical and chemical structure of SVS13-A, which is composed by a hot corino and an envelope extending up to ~ 7000 au in radius. The envelope has an increasing density and temperature going inward. From a chemical point of view, the outermost region is probed by HC_3N emission, then by H_2CO , and finally by H_2CS .

- The DC₃N/HC₃N abundance ratio decreases going inward whereas that of HDCS/H₂CS increases. We explained this behavior with the different chemical formation of cyanoacetylene and thioformaldehyde: the former is a present-day gas-phase product whereas the latter is a past grain-surface product.

Obviously, more observations of Class I protostars are necessary to draw a reliable picture of the chemical evolution during the solar-type formation process. This means not only a much larger number of sources, but also better accuracy and spatial resolution, so to be able to disentangle the various components making a Class I protostar. Some observational programs are already in progress, like the IRAM-NOEMA Large Program SOLIS (*Seeds Of Life In Space*)³ and the ALMA Large Program FAUST (Fifty AU Study of the chemistry in the disk/envelope system of Solar-like protostars; <http://stars.riken.jp/faust/fausthome.html>, PI: Yamamoto). Both projects aim at collecting much more observational data towards Class I protostars, in addition to other sources in different evolutionary phases.

In addition, an important question remains about the opacity of the iCOMs line in the millimeter, which affects their abundance measure. An illustrative example of this problem is represented by the HH212 Class 0 protostar, which was imaged with ALMA with a resolution of 10 au^{166–168}. While iCOMs are detected in the upper atmosphere of its circumstellar disk, no emission is found towards the denser disk midplane¹⁶⁹. The question is: is the lack of iCOMs emission towards the midplane due to an intrinsic small abundance or is it caused by a high continuum optical depth? To answer this question observations in the cm-domain are needed. Therefore, the future SKA telescope will be instrumental in this respect (see e.g. Cradle of Life¹⁷⁰ at <https://astronomers.skatelescope.org/science-working-groups/galaxy-cradle-life/>).

We would also like to emphasize the importance of the synergy between astronomers and chemists for the interpretation of observations. The case of H₂CS described in Section 5 provides an illustrative example on the necessity to have laboratory experiments and theoretical quantum chemistry calculations in order to be able to draw firm conclusions from the astronomical observations. We can mention the large-scale project ACO (Astro-Chemical Origins: <https://aco->

itn.oapd.inaf.it/home, PI: Ceccarelli, grant No 811312), funded by the European Commission, which gathers together instrumentalists, astronomers, chemists and computer scientists.

Acknowledgement

This work is based on observations carried out with the IRAM-NOEMA Interferometer and IRAM-30m telescope. IRAM is supported by INSU/CNRS (France), MPG (Germany) and IGN (Spain). This project has received funding from (i) the European Research Council (ERC) under the European Union's Horizon 2020 research and innovation programme, for the Project "The Dawn of Organic Chemistry" (DOC), grant agreement No 741002 and (ii) the European MARIE SKŁODOWSKA-CURIE ACTIONS under the European Union's Horizon 2020 research and innovation programme, for the Project "Astro-Chemistry Origins" (ACO), Grant No 811312. This work was supported by the PRIN-INAF 2016 "The Cradle of Life - GENESIS-SKA (General Conditions in Early Planetary Systems for the rise of life with SKA)".

References

- (1) McGuire, B. A. 2018 Census of Interstellar, Circumstellar, Extragalactic, Protoplanetary Disk, and Exoplanetary Molecules. *ApJS* **2018**, 239, 17.
- (2) Herbst, E.; van Dishoeck, E. F. Complex Organic Interstellar Molecules. *ARA&A* **2009**, 47, 427–480.
- (3) Ceccarelli, C. et al. Seeds Of Life In Space (SOLIS): The Organic Composition Diversity at 300-1000 au Scale in Solar-type Star-forming Regions. *ApJ* **2017**, 850, 176.
- (4) Ceccarelli, C.; Caselli, P.; Bockelée-Morvan, D.; Mousis, O.; Pizzarello, S.; Robert, F.; Semenov, D. Deuterium Fractionation: The Ariadne's Thread from the Precollapse Phase to Meteorites and Comets Today. *Protostars and Planets VI* **2014**, 859–882.

- (5) Caselli, P.; Ceccarelli, C. Our Astrochemical Heritage. *A&A Rev.* **2012**, *20*, 56.
- (6) Bianchi, E.; Codella, C.; Ceccarelli, C.; Fontani, F.; Testi, L.; Bachiller, R.; Lefloch, B.; Podio, L.; Taquet, V. Decrease of the Organic Deuteration during the Evolution of Sun-like Protostars: the Case of SVS13-A. *MNRAS* **2017**, *467*, 3011–3023.
- (7) Bianchi, E.; Codella, C.; Ceccarelli, C.; Vazart, F.; Bachiller, R.; Balucani, N.; Bouvier, M.; De Simone, M.; Enrique-Romero, J.; Kahane, C.; Lefloch, B.; López-Sepulcre, A.; Ospina-Zamudio, J.; Podio, L.; Taquet, V. The Census of Interstellar Complex Organic Molecules in the Class I Hot Corino of SVS13-A. *MNRAS* **2019**, *483*, 1850–1861.
- (8) Shu, F. H. Self-similar Collapse of Isothermal Spheres and Star Formation. *ApJ* **1977**, *214*, 488–497.
- (9) Shu, F. H.; Adams, F. C. Star Formation and the Circumstellar Matter of Young Stellar Objects. *Circumstellar Matter*. 1987; pp 7–22.
- (10) Galli, D.; Lizano, S.; Shu, F. H.; Allen, A. Gravitational Collapse of Magnetized Clouds. I. Ideal Magnetohydrodynamic Accretion Flow. *ApJ* **2006**, *647*, 374–381.
- (11) Hennebelle, P.; Teyssier, R. Magnetic Processes in a Collapsing Dense Core. II. Fragmentation. Is there a Fragmentation Crisis? *A&A* **2008**, *477*, 25–34.
- (12) André, P.; Di Francesco, J.; Ward-Thompson, D.; Inutsuka, S.-I.; Pudritz, R. E.; Pineda, J. E. From Filamentary Networks to Dense Cores in Molecular Clouds: Toward a New Paradigm for Star Formation. *Protostars and Planets VI* **2014**, 27–51.
- (13) Klessen, R. S.; Glover, S. C. O. Physical Processes in the Interstellar Medium. *Star Formation in Galaxy Evolution: Connecting Numerical Models to Reality, Saas-Fee Advanced Course, Volume 43*. ISBN 978-3-662-47889-9. Springer-Verlag Berlin Heidelberg, 2016, p. 85 **2016**, *43*, 85.

- (14) Dunham, M. M.; Stutz, A. M.; Allen, L. E.; Evans, N. J., II; Fischer, W. J.; Megeath, S. T.; Myers, P. C.; Offner, S. S. R.; Poteet, C. A.; Tobin, J. J.; Vorobyov, E. I. The Evolution of Protostars: Insights from Ten Years of Infrared Surveys with Spitzer and Herschel. *Protostars and Planets VI* **2014**, 195–218.
- (15) Persson, M. V. SEDs of the different protostellar evolutionary stages. 2014; https://figshare.com/articles/SEDs_of_the_different_protostellar_evolutionary_stages/1121574.
- (16) Lee, C.-F.; Ho, P. T. P.; Li, Z.-Y.; Hirano, N.; Zhang, Q.; Shang, H. A Rotating Protostellar Jet Launched from the Innermost Disk of HH 212. *Nature Astronomy* **2017**, *1*, 0152.
- (17) Marois, C.; Zuckerman, B.; Konopacky, Q. M.; Macintosh, B.; Barman, T. Images of a Fourth Planet Orbiting HR 8799. *Nature* **2010**, *468*, 1080–1083.
- (18) Müller, A. et al. Orbital and Atmospheric Characterization of the Planet within the Gap of the PDS 70 Transition Disk. *A&A* **2018**, *617*, L2.
- (19) Suriano, S. S.; Li, Z.-Y.; Krasnopolsky, R.; Shang, H. The formation of rings and gaps in magnetically coupled disc-wind systems: ambipolar diffusion and reconnection. *MNRAS* **2018**, *477*, 1239–1257.
- (20) Barge, P.; Ricci, L.; Carilli, C. L.; Previn-Ratnasingam, R. Gaps and rings carved by vortices in protoplanetary dust. *A&A* **2017**, *605*, A122.
- (21) Ruge, J. P.; Flock, M.; Wolf, S.; Dzyurkevich, N.; Fromang, S.; Henning, T.; Klahr, H.; Meheut, H. Gaps, rings, and non-axisymmetric structures in protoplanetary disks: Emission from large grains. *A&A* **2016**, *590*, A17.
- (22) Zhang, K.; Blake, G.; Bergin, E. Evidence of fast pebble growth near condensation fronts in the HL Tau protoplanetary disk. IAU General Assembly. 2015; p 2256118.

- (23) Gonzalez, J. F.; Laibe, G.; Maddison, S. T.; Pinte, C.; Ménard, F. ALMA images of discs: are all gaps carved by planets? *MNRAS* **2015**, *454*, L36–L40.
- (24) Flock, M.; Ruge, J. P.; Dzyurkevich, N.; Henning, T.; Klahr, H.; Wolf, S. Gaps, rings, and non-axisymmetric structures in protoplanetary disks. From simulations to ALMA observations. *A&A* **2015**, *574*, A68.
- (25) Ober, F.; Wolf, S.; Uribe, A. L.; Klahr, H. H. Tracing Planet-induced Structures in Circumstellar Disks using Molecular Lines. *A&A* **2015**, *579*, A105.
- (26) Baruteau, C.; Bai, X.; Mordasini, C.; Mollière, P. Formation, Orbital and Internal Evolutions of Young Planetary Systems. *Space Sci. Rev.* **2016**, *205*, 77–124.
- (27) Facchini, S.; Pinilla, P.; van Dishoeck, E. F.; de Juan Ovelar, M. Inferring Giant Planets from ALMA Millimeter Continuum and Line Observations in (Transition) Disks. *A&A* **2018**, *612*, A104.
- (28) Andrews, S. M.; Wilner, D. J.; Zhu, Z.; Birnstiel, T.; Carpenter, J. M.; Pérez, L. M.; Bai, X.-N.; Öberg, K. I.; Hughes, A. M.; Isella, A.; Ricci, L. Ringed Substructure and a Gap at 1 au in the Nearest Protoplanetary Disk. *ApJ* **2016**, *820*, L40.
- (29) Isella, A.; Turner, N. J. Signatures of Young Planets in the Continuum Emission from Protoplanetary Disks. *The Astrophysical Journal* **2018**, *860*, 27.
- (30) Fedele, D.; Carney, M.; Hogerheijde, M. R.; Walsh, C.; Miotello, A.; Klaassen, P.; Bruderer, S.; Henning, T.; van Dishoeck, E. F. ALMA Unveils Rings and Gaps in the Protoplanetary System HD 169142: Signatures of Two Giant Protoplanets. *A&A* **2017**, *600*, A72.
- (31) Loomis, R. A.; Öberg, K. I.; Andrews, S. M.; MacGregor, M. A. A Multi-ringed, Modestly Inclined Protoplanetary Disk around AA Tau. *ApJ* **2017**, *840*, 23.
- (32) Andrews, S. M. et al. The Disk Substructures at High Angular Resolution Project (DSHARP). I. Motivation, Sample, Calibration, and Overview. *ApJ* **2018**, *869*, L41.

- (33) Dipierro, G. et al. Rings and Gaps in the Disc around Elias 24 Revealed by ALMA. *MNRAS* **2018**, 475, 5296–5312.
- (34) van der Marel, N.; Dong, R.; di Francesco, J.; Williams, J. P.; Tobin, J. Protoplanetary Disk Rings and Gaps across Ages and Luminosities. *ApJ* **2019**, 872, 112.
- (35) Favre, C.; Fedele, D.; Maud, L.; Booth, R.; Tazzari, M.; Miotello, A.; Testi, L.; Semenov, D.; Bruderer, S. Gas Density Perturbations Induced by One or More Forming Planets in the AS 209 Protoplanetary Disk as Seen with ALMA. *ApJ* **2019**, 871, 107.
- (36) Teague, R.; Bae, J.; Birnstiel, T.; Bergin, E. A. Evidence for a Vertical Dependence on the Pressure Structure in AS 209. *ApJ* **2018**, 868, 113.
- (37) Pinte, C.; Price, D. J.; Ménard, F.; Duchêne, G.; Dent, W. R. F.; Hill, T.; de Gregorio-Monsalvo, I.; Hales, A.; Mentiplay, D. Kinematic Evidence for an Embedded Protoplanet in a Circumstellar Disk. *ApJ* **2018**, 860, L13.
- (38) ALMA Partnership, et al. The 2014 ALMA Long Baseline Campaign: First Results from High Angular Resolution Observations toward the HL Tau Region. *ApJ* **2015**, 808, L3.
- (39) Dong, R.; Zhu, Z.; Whitney, B. Observational Signatures of Planets in Protoplanetary Disks I. Gaps Opened by Single and Multiple Young Planets in Disks. *ApJ* **2015**, 809, 93.
- (40) Evans, N. J., II et al. The Spitzer c2d Legacy Results: Star-Formation Rates and Efficiencies; Evolution and Lifetimes. *ApJS* **2009**, 181, 321–350.
- (41) Sheehan, P. D.; Eisner, J. A. Disk Masses for Embedded Class I Protostars in the Taurus Molecular Cloud. *ApJ* **2017**, 851, 45.
- (42) Andersen, B. C.; Stephens, I. W.; Dunham, M. M.; Pokhrel, R.; Jørgensen, J. K.; Frimann, S.; Segura-Cox, D.; Myers, P. C.; Bourke, T. L.; Tobin, J. J.; Tychoniec, Ł. The Mass Evolution of Protostellar Disks and Envelopes in the Perseus Molecular Cloud. *The Astrophysical Journal* **2019**, 873, 54.

- (43) Yamamoto, S. *Introduction to Astrochemistry: Chemical Evolution from Interstellar Clouds to Star and Planet Formation*, *Astronomy and Astrophysics Library*, by Satoshi Yamamoto. ISBN 978-4-431-54170-7. Springer Japan, 2017; 2017.
- (44) Watanabe, N.; Kouchi, A. Efficient Formation of Formaldehyde and Methanol by the Addition of Hydrogen Atoms to CO in H₂O-CO Ice at 10 K. *ApJ* **2002**, *571*, L173–L176.
- (45) Rimola, A.; Taquet, V.; Ugliengo, P.; Balucani, N.; Ceccarelli, C. Combined Quantum Chemical and Modeling Study of CO Hydrogenation on Water Ice. *A&A* **2014**, *572*, A70.
- (46) Boogert, A. C. A.; Gerakines, P. A.; Whittet, D. C. B. Observations of the Icy Universe. *ARA&A* **2015**, *53*, 541–581.
- (47) Öberg, K. I.; Bottinelli, S.; Jørgensen, J. K.; van Dishoeck, E. F. A Cold Complex Chemistry Toward the Low-mass Protostar B1-b: Evidence for Complex Molecule Production in Ices. *ApJ* **2010**, *716*, 825–834.
- (48) Bacmann, A.; Taquet, V.; Faure, A.; Kahane, C.; Ceccarelli, C. Detection of Complex Organic Molecules in a Prestellar Core: a New Challenge for Astrochemical Models. *A&A* **2012**, *541*, L12.
- (49) Cernicharo, J.; Marcelino, N.; Roueff, E.; Gerin, M.; Jiménez-Escobar, A.; Muñoz Caro, G. M. Discovery of the Methoxy Radical, CH₃O, toward B1: Dust Grain and Gas-phase Chemistry in Cold Dark Clouds. *ApJ* **2012**, *759*, L43.
- (50) Vastel, C.; Ceccarelli, C.; Lefloch, B.; Bachiller, R. The Origin of Complex Organic Molecules in Prestellar Cores. *ApJ* **2014**, *795*, L2.
- (51) Jiménez-Serra, I.; Vasyunin, A. I.; Caselli, P.; Marcelino, N.; Billot, N.; Viti, S.; Testi, L.; Vastel, C.; Lefloch, B.; Bachiller, R. The Spatial Distribution of Complex Organic Molecules in the L1544 Pre-stellar Core. *ApJ* **2016**, *830*, L6.

- (52) Punanova, A. et al. Seeds of Life in Space (SOLIS). III. Zooming Into the Methanol Peak of the Prestellar Core L1544. *ApJ* **2018**, 855, 112.
- (53) Vasyunin, A. I.; Herbst, E. Reactive Desorption and Radiative Association as Possible Drivers of Complex Molecule Formation in the Cold Interstellar Medium. *ApJ* **2013**, 769, 34.
- (54) Balucani, N.; Ceccarelli, C.; Taquet, V. Formation of complex organic molecules in cold objects: the role of gas-phase reactions. *MNRAS* **2015**, 449, L16–L20.
- (55) Cazaux, S.; Tielens, A. G. G. M.; Ceccarelli, C.; Castets, A.; Wakelam, V.; Caux, E.; Parise, B.; Teyssier, D. The Hot Core around the Low-mass Protostar IRAS 16293-2422: Scoundrels Rule! *ApJ* **2003**, 593, L51–L55.
- (56) Taquet, V.; López-Sepulcre, A.; Ceccarelli, C.; Neri, R.; Kahane, C.; Charnley, S. B. Constraining the Abundances of Complex Organics in the Inner Regions of Solar-type Protostars. *ApJ* **2015**, 804, 81.
- (57) Jørgensen, J. K. et al. The ALMA Protostellar Interferometric Line Survey (PILS). First Results from an Unbiased Submillimeter Wavelength Line Survey of the Class 0 Protostellar Binary IRAS 16293-2422 with ALMA. *A&A* **2016**, 595, A117.
- (58) Calcutt, H.; Fiechter, M. R.; Willis, E. R.; Müller, H. S. P.; Garrod, R. T.; Jørgensen, J. K.; Wampfler, S. F.; Bourke, T. L.; Coutens, A.; Drozdovskaya, M. N.; Ligterink, N. F. W.; Kristensen, L. E. The ALMA-PILS Survey: First Detection of Methyl Isocyanide (CH_3NC) in a Solar-type Protostar. *A&A* **2018**, 617, A95.
- (59) Garrod, R. T.; Herbst, E. Formation of Methyl Formate and Other Organic Species in the Warm-up Phase of Hot Molecular Cores. *A&A* **2006**, 457, 927–936.
- (60) Garrod, R. T.; Widicus Weaver, S. L.; Herbst, E. Complex Chemistry in Star-forming Regions: An Expanded Gas-Grain Warm-up Chemical Model. *ApJ* **2008**, 682, 283–302.

- (61) Rimola, A.; Skouteris, D.; Balucani, N.; Ceccarelli, C.; Enrique-Romero, J.; Taquet, V.; Ugliengo, P. Can Formamide Be Formed on Interstellar Ice? An Atomistic Perspective. *ACS Earth and Space Chemistry*, vol. 2, issue 7, pp. 720-734 **2018**, 2, 720–734.
- (62) Enrique-Romero, J.; Rimola, A.; Ceccarelli, C.; Ugliengo, P.; Balucani, N.; Skouteris, D. Reactivity of HCO with CH₃ and NH₂ on Water Ice Surfaces. A Comprehensive Accurate Quantum Chemistry Study. *ACS Earth and Space Chemistry* **2019**, 3, 2158–2170.
- (63) Skouteris, D.; Vazart, F.; Ceccarelli, C.; Balucani, N.; Puzzarini, C.; Barone, V. New Quantum Chemical Computations of Formamide Deuteration Support Gas-phase Formation of this Prebiotic Molecule. *MNRAS* **2017**, 468, L1–L5.
- (64) Skouteris, D.; Balucani, N.; Ceccarelli, C.; Vazart, F.; Puzzarini, C.; Barone, V.; Codella, C.; Lefloch, B. The Genealogical Tree of Ethanol: Gas-phase Formation of Glycolaldehyde, Acetic Acid, and Formic Acid. *ApJ* **2018**, 854, 135.
- (65) Skouteris, D.; Balucani, N.; Ceccarelli, C.; Faginas Lago, N.; Codella, C.; Falcinelli, S.; Rosi, M. Interstellar Dimethyl Ether Gas-phase Formation: a Quantum Chemistry and Kinetics Study. *MNRAS* **2019**, 482, 3567–3575.
- (66) Öberg, K. I.; Guzmán, V. V.; Furuya, K.; Qi, C.; Aikawa, Y.; Andrews, S. M.; Loomis, R.; Wilner, D. J. The Comet-like Composition of a Protoplanetary Disk as Revealed by Complex Cyanides. *Nature* **2015**, 520, 198–201.
- (67) Bergner, J. B.; Guzmán, V. G.; Öberg, K. I.; Loomis, R. A.; Pegues, J. A Survey of CH₃CN and HC₃N in Protoplanetary Disks. *ApJ* **2018**, 857, 69.
- (68) Favre, C. et al. First Detection of the Simplest Organic Acid in a Protoplanetary Disk. *ApJ* **2018**, 862, L2.
- (69) Le Roy, L. et al. Inventory of the Volatiles on Comet 67P/Churyumov-Gerasimenko from Rosetta/ROSINA. *A&A* **2015**, 583, A1.

- (70) Drozdovskaya, M. N.; van Dishoeck, E. F.; Jørgensen, J. K.; Calmonte, U.; van der Wiel, M. H. D.; Coutens, A.; Calcutt, H.; Müller, H. S. P.; Bjerkeli, P.; Persson, M. V.; Wampfler, S. F.; Altwegg, K. The ALMA-PILS Survey: the Sulphur Connection between Protostars and Comets: IRAS 16293-2422 B and 67P/Churyumov-Gerasimenko. *MNRAS* **2018**, *476*, 4949–4964.
- (71) Linsky, J. L. et al. What Is the Total Deuterium Abundance in the Local Galactic Disk? *ApJ* **2006**, *647*, 1106–1124.
- (72) Parise, B.; Castets, A.; Herbst, E.; Caux, E.; Ceccarelli, C.; Mukhopadhyay, I.; Tielens, A. G. G. M. First Detection of Triply-deuterated Methanol. *A&A* **2004**, *416*, 159–163.
- (73) Bacmann, A.; Lefloch, B.; Ceccarelli, C.; Steinacker, J.; Castets, A.; Loinard, L. CO Depletion and Deuterium Fractionation in Prestellar Cores. *ApJ* **2003**, *585*, L55–L58.
- (74) Vastel, C.; Phillips, T. G.; Ceccarelli, C.; Pearson, J. First Detection of Doubly Deuterated Hydrogen Sulfide. *ApJ* **2003**, *593*, L97–L100.
- (75) Vastel, C.; Phillips, T. G.; Yoshida, H. Detection of D_2H^+ in the Dense Interstellar Medium. *ApJ* **2004**, *606*, L127–L130.
- (76) Vastel, C.; Caselli, P.; Ceccarelli, C.; Phillips, T.; Wiedner, M. C.; Peng, R.; Houde, M.; Dominik, C. The Distribution of Ortho- $H_2D^+(1_{1,0}-1_{1,1})$ in L1544: Tracing the Deuteration Factory in Prestellar Cores. *ApJ* **2006**, *645*, 1198–1211.
- (77) Bizzocchi, L.; Caselli, P.; Spezzano, S.; Leonardo, E. Deuterated Methanol in the Pre-stellar Core L1544. *A&A* **2014**, *569*, A27.
- (78) Chacón-Tanarro, A.; Caselli, P.; Bizzocchi, L.; Pineda, J. E.; Sipilä, O.; Vasyunin, A.; Spezzano, S.; Punanova, A.; Giuliano, B. M.; Lattanzi, V. Mapping Deuterated Methanol toward L1544. I. Deuterium Fraction and Comparison with Modeling. *A&A* **2019**, *622*, A141.

- (79) Ceccarelli, C.; Loinard, L.; Castets, A.; Tielens, A. G. G. M.; Caux, E.; Lefloch, B.; Vastel, C. Extended D₂CO Emission: the Smoking Gun of Grain Surface-chemistry. *A&A* **2001**, 372, 998–1004.
- (80) Parise, B.; Ceccarelli, C.; Tielens, A. G. G. M.; Herbst, E.; Lefloch, B.; Caux, E.; Castets, A.; Mukhopadhyay, I.; Pagani, L.; Loinard, L. Detection of Doubly-deuterated Methanol in the Solar-type Protostar IRAS 16293-2422. *A&A* **2002**, 393, L49–L53.
- (81) Parise, B.; Ceccarelli, C.; Tielens, A. G. G. M.; Castets, A.; Caux, E.; Lefloch, B.; Maret, S. Testing Grain Surface Chemistry: a Survey of Deuterated Formaldehyde and Methanol in Low-mass Class 0 Protostars. *A&A* **2006**, 453, 949–958.
- (82) Coutens, A. et al. The ALMA-PILS Survey: First Detections of Deuterated Formamide and Deuterated Isocyanic Acid in the Interstellar Medium. *A&A* **2016**, 590, L6.
- (83) Manigand, S.; Calcutt, H.; Jørgensen, J. K.; Taquet, V.; Müller, H. S. P.; Coutens, A.; Wampfler, S. F.; Ligterink, N. F. W.; Drozdovskaya, M. N.; Kristensen, L. E.; van der Wiel, M. H. D.; Bourke, T. L. The ALMA-PILS Survey: the First Detection of Doubly Deuterated Methyl Formate (CHD₂OCHO) in the ISM. *A&A* **2019**, 623, A69.
- (84) van Dishoeck, E. F.; Thi, W.-F.; van Zadelhoff, G.-J. Detection of DCO⁺ in a Circumstellar Disk. *A&A* **2003**, 400, L1–L4.
- (85) Guilloteau, S.; Piétu, V.; Dutrey, A.; Guélin, M. Deuterated Molecules in DM Tauri: DCO⁺, but no HDO. *A&A* **2006**, 448, L5–L8.
- (86) Öberg, K. I.; Qi, C.; Wilner, D. J.; Hogerheijde, M. R. Evidence for Multiple Pathways to Deuterium Enhancements in Protoplanetary Disks. *ApJ* **2012**, 749, 162.
- (87) Huang, J.; Öberg, K. I.; Qi, C.; Aikawa, Y.; Andrews, S. M.; Furuya, K.; Guzmán, V. V.; Loomis, R. A.; van Dishoeck, E. F.; Wilner, D. J. An ALMA Survey of DCN/H¹³CN and DCO⁺/H¹³CO⁺ in Protoplanetary Disks. *ApJ* **2017**, 835, 231.

- (88) Teague, R.; Semenov, D.; Guilloteau, S.; Henning, T.; Dutrey, A.; Wakelam, V.; Chapillon, E.; Pietu, V. Chemistry in Disks. IX. Observations and Modelling of HCO^+ and DCO^+ in DM Tauri. *A&A* **2015**, *574*, A137.
- (89) Salinas, V. N.; Hogerheijde, M. R.; Mathews, G. S.; Öberg, K. I.; Qi, C.; Williams, J. P.; Wilner, D. J. DCO^+ , DCN , and N_2D^+ Reveal Three Different Deuteration Regimes in the Disk around the Herbig Ae Star HD 163296. *A&A* **2017**, *606*, A125.
- (90) Mathews, G. S.; Klaassen, P. D.; Juhász, A.; Harsono, D.; Chapillon, E.; van Dishoeck, E. F.; Espada, D.; de Gregorio-Monsalvo, I.; Hales, A.; Hogerheijde, M. R.; Mottram, J. C.; Rawlings, M. G.; Takahashi, S.; Testi, L. ALMA Imaging of the CO Snowline of the HD 163296 Disk with DCO^+ . *A&A* **2013**, *557*, A132.
- (91) Öberg, K. I.; Qi, C.; Fogel, J. K. J.; Bergin, E. A.; Andrews, S. M.; Espaillat, C.; Wilner, D. J.; Pascucci, I.; Kastner, J. H. Disk Imaging Survey of Chemistry with SMA. II. Southern Sky Protoplanetary Disk Data and Full Sample Statistics. *ApJ* **2011**, *734*, 98.
- (92) Qi, C.; Wilner, D. J.; Aikawa, Y.; Blake, G. A.; Hogerheijde, M. R. Resolving the Chemistry in the Disk of TW Hydrae. I. Deuterated Species. *ApJ* **2008**, *681*, 1396–1407.
- (93) Qi, C.; Öberg, K. I.; Andrews, S. M.; Wilner, D. J.; Bergin, E. A.; Hughes, A. M.; Hogerheijde, M.; D’Alessio, P. Chemical Imaging of the CO Snow Line in the HD 163296 Disk. *ApJ* **2015**, *813*, 128.
- (94) Spezzano, S.; Brünken, S.; Schilke, P.; Caselli, P.; Menten, K. M.; McCarthy, M. C.; Bizzocchi, L.; Treviño-Morales, S. P.; Aikawa, Y.; Schlemmer, S. Interstellar Detection of $c\text{-C}_3\text{D}_2$. *ApJ* **2013**, *769*, L19.
- (95) Taquet, V.; Peters, P. S.; Kahane, C.; Ceccarelli, C.; López-Sepulcre, A.; Toubin, C.; Duflot, D.; Wiesenfeld, L. Water Ice Deuteration: a Tracer of the Chemical History of Protostars. *A&A* **2013**, *550*, A127.

- (96) Coutens, A.; Vastel, C.; Caux, E.; Ceccarelli, C.; Bottinelli, S.; Wiesenfeld, L.; Faure, A.; Scribano, Y.; Kahane, C. A Study of Deuterated Water in the Low-mass Protostar IRAS 16293-2422. *A&A* **2012**, 539, A132.
- (97) Persson, M. V.; Jørgensen, J. K.; van Dishoeck, E. F.; Harsono, D. The deuterium fractionation of water on solar-system scales in deeply-embedded low-mass protostars. *A&A* **2014**, 563, A74.
- (98) Jensen, S. S.; Jørgensen, J. K.; Kristensen, L. E.; Furuya, K.; Coutens, A.; van Dishoeck, E. F.; Harsono, D.; Persson, M. V. ALMA observations of water deuteration: a physical diagnostic of the formation of protostars. *A&A* **2019**, 631, A25.
- (99) Persson, M. V.; Jørgensen, J. K.; Müller, H. S. P.; Coutens, A.; van Dishoeck, E. F.; Taquet, V.; Calcutt, H.; van der Wiel, M. H. D.; Bourke, T. L.; Wampfler, S. F. The ALMA-PILS Survey: Formaldehyde Deuteration in Warm Gas on Small Scales toward IRAS 16293-2422 B. *A&A* **2018**, 610, A54.
- (100) Jørgensen, J. K.; Müller, H. S. P.; Calcutt, H.; Coutens, A.; Drozdovskaya, M. N.; Öberg, K. I.; Persson, M. V.; Taquet, V.; van Dishoeck, E. F.; Wampfler, S. F. The ALMA-PILS Survey: Isotopic Composition of Oxygen-containing Complex Organic Molecules toward IRAS 16293-2422B. *A&A* **2018**, 620, A170.
- (101) Bianchi, E., et al. Deuterated Methanol on a Solar System Scale around the HH212 Protostar. *A&A* **2017**, 606, L7.
- (102) Codella, C.; Ceccarelli, C.; Lefloch, B.; Fontani, F.; Busquet, G.; Caselli, P.; Kahane, C.; Lis, D.; Taquet, V.; Vasta, M.; Viti, S.; Wiesenfeld, L. The Herschel and IRAM CHESSE Spectral Surveys of the Protostellar Shock L1157-B1: Fossil Deuteration. *ApJ* **2012**, 757, L9.
- (103) Fontani, F.; Codella, C.; Ceccarelli, C.; Lefloch, B.; Viti, S.; Benedettini, M. The L1157-

- B1 Astrochemical Laboratory: Measuring the True Formaldehyde Deuteration on Grain Mantles. *ApJ* **2014**, 788, L43.
- (104) Codella, C.; Ceccarelli, C.; Bianchi, E.; Podio, L.; Bachiller, R.; Lefloch, B.; Fontani, F.; Taquet, V.; Testi, L. Hot and dense water in the inner 25 au of SVS13-A. *MNRAS* **2016**, 462, L75–L79.
- (105) Watson, W. D. Ion-Molecule Reactions, Molecule Formation, and Hydrogen-Isotope Exchange in Dense Interstellar Clouds. *ApJ* **1974**, 188, 35–42.
- (106) Roberts, H.; Millar, T. J. Gas-phase Formation of Doubly-deuterated Species. *A&A* **2000**, 364, 780–784.
- (107) Flower, D. R.; Pineau Des Forêts, G.; Walmsley, C. M. The Importance of the Ortho:Para H₂ Ratio for the Deuteration of Molecules during Pre-protostellar Collapse. *A&A* **2006**, 449, 621–629.
- (108) Bovino, S.; Grassi, T.; Schleicher, D. R. G.; Caselli, P. H₂ Ortho-to-para Conversion on Grains: A Route to Fast Deuterium Fractionation in Dense Cloud Cores? *ApJ* **2017**, 849, L25.
- (109) Taquet, V.; Ceccarelli, C.; Kahane, C. Formaldehyde and Methanol Deuteration in Protostars: Fossils from a Past Fast High-density Pre-collapse Phase. *ApJ* **2012**, 748, L3.
- (110) Cleaves, L. I.; Bergin, E. A.; Alexander, C. M. O. .; Du, F.; Graninger, D.; Öberg, K. I.; Harries, T. J. The Ancient Heritage of Water Ice in the Solar System. *Science* **2014**, 345, 1590–1593.
- (111) Furuya, K.; van Dishoeck, E. F.; Aikawa, Y. Reconstructing the History of Water Ice Formation from HDO/H₂O and D₂O/HDO Ratios in Protostellar Cores. *A&A* **2016**, 586, A127.
- (112) Furuya, K.; Drozdovskaya, M. N.; Visser, R.; van Dishoeck, E. F.; Walsh, C.; Harsono, D.;

- Hincelin, U.; Taquet, V. Water Delivery from Cores to Disks: Deuteration as a Probe of the Prestellar Inheritance of H₂O. *A&A* **2017**, 599, A40.
- (113) Caux, E. et al. TIMASSS: the IRAS 16293-2422 Millimeter and Submillimeter Spectral Survey. I. Observations, Calibration, and Analysis of the Line Kinematics. *A&A* **2011**, 532, A23.
- (114) Bottinelli, S.; Ceccarelli, C.; Lefloch, B.; Williams, J. P.; Castets, A.; Caux, E.; Cazaux, S.; Maret, S.; Parise, B.; Tielens, A. G. G. M. Complex Molecules in the Hot Core of the Low-Mass Protostar NGC 1333 IRAS 4A. *ApJ* **2004**, 615, 354–358.
- (115) Maret, S.; Ceccarelli, C.; Tielens, A. G. G. M.; Caux, E.; Lefloch, B.; Faure, A.; Castets, A.; Flower, D. R. CH₃OH Abundance in Low Mass Protostars. *A&A* **2005**, 442, 527–538.
- (116) Bottinelli, S.; Ceccarelli, C.; Williams, J. P.; Lefloch, B. Hot corinos in NGC 1333-IRAS4B and IRAS2A. *A&A* **2007**, 463, 601–610.
- (117) Öberg, K. I.; van der Marel, N.; Kristensen, L. E.; van Dishoeck, E. F. Complex Molecules toward Low-mass Protostars: The Serpens Core. *ApJ* **2011**, 740, 14.
- (118) Öberg, K. I.; Lauck, T.; Graninger, D. Complex Organic Molecules during Low-mass Star Formation: Pilot Survey Results. *ApJ* **2014**, 788, 68.
- (119) Graninger, D. M.; Wilkins, O. H.; Öberg, K. I. Carbon Chains and Methanol toward Embedded Protostars. *ApJ* **2016**, 819, 140.
- (120) Lefloch, B. et al. Astrochemical Evolution along Star Formation: Overview of the IRAM Large Program ASAI. *MNRAS* **2018**, 477, 4792–4809.
- (121) Bergner, J. B.; Öberg, K. I.; Garrod, R. T.; Graninger, D. M. Complex Organic Molecules toward Embedded Low-mass Protostars. *ApJ* **2017**, 841, 120.
- (122) Law, C. J.; Öberg, K. I.; Bergner, J. B.; Graninger, D. Carbon Chain Molecules toward Embedded Low-mass Protostars. *ApJ* **2018**, 863, 88.

- (123) De Simone, M.; Codella, C.; Testi, L.; Belloche, A.; Maury, A. J.; Anderl, S.; André, P.; Maret, S.; Podio, L. Glycolaldehyde in Perseus Young Solar Analogs. *A&A* **2017**, *599*, A121.
- (124) Codella, C. et al. The CHESSE Spectral Survey of Star Forming Regions: Peering into the Protostellar Shock L1157-B1. I. Shock Chemical Complexity. *A&A* **2010**, *518*, L112.
- (125) Lefloch, B.; Ceccarelli, C.; Codella, C.; Favre, C.; Podio, L.; Vastel, C.; Viti, S.; Bachiller, R. L1157-B1, a Factory of Complex Organic Molecules in a Solar-type Star-forming Region. *MNRAS* **2017**, *469*, L73–L77.
- (126) Bergner, J. B.; Martín-Doménech, R.; Öberg, K. I.; Jørgensen, J. K.; Artur de la Villar-mois, E.; Brinch, C. Organic Complexity in Protostellar Disk Candidates. *ACS Earth and Space Chemistry*, vol. 3, issue 8, pp. 1564-1575 **2019**, *3*, 1564–1575.
- (127) Pezzuto, S. et al. Herschel Observations of B1-bS and B1-bN: Two First Hydrostatic Core Candidates in the Perseus Star-forming Cloud. *A&A* **2012**, *547*, A54.
- (128) Gerin, M.; Pety, J.; Fuente, A.; Cernicharo, J.; Commerçon, B.; Marcelino, N. Nascent Bipolar Outflows Associated with the First Hydrostatic Core Candidates Barnard 1b-N and 1b-S. *A&A* **2015**, *577*, L2.
- (129) López-Sepulcre, A. et al. Complex organics in IRAS 4A revisited with ALMA and PdBI: Striking contrast between two neighbouring protostellar cores. *A&A* **2017**, *606*, A121.
- (130) Jaber, A. A.; Ceccarelli, C.; Kahane, C.; Caux, E. The Census of Complex Organic Molecules in the Solar-type Protostar IRAS16293-2422. *ApJ* **2014**, *791*, 29.
- (131) Imai, M.; Sakai, N.; Oya, Y.; López-Sepulcre, A.; Watanabe, Y.; Ceccarelli, C.; Lefloch, B.; Caux, E.; Vastel, C.; Kahane, C.; Sakai, T.; Hirota, T.; Aikawa, Y.; Yamamoto, S. Discovery of a Hot Corino in the Bok Globule B335. *ApJ* **2016**, *830*, L37.

- (132) Oya, Y.; Sakai, N.; Watanabe, Y.; Higuchi, A. E.; Hirota, T.; López-Sepulcre, A.; Sakai, T.; Aikawa, Y.; Ceccarelli, C.; Lefloch, B.; Caux, E.; Vastel, C.; Kahane, C.; Yamamoto, S. L483: Warm Carbon-chain Chemistry Source Harboring Hot Corino Activity. *ApJ* **2017**, 837, 174.
- (133) Loinard, L.; Castets, A.; Ceccarelli, C.; Lefloch, B.; Benayoun, J.-J.; Caux, E.; Vastel, C.; Dartois, E.; Tielens, A. G. G. M. Doubly Deuterated Formaldehyde in Star-forming Regions: an Observational Approach. *Planet. Space Sci.* **2002**, 50, 1205–1213.
- (134) Roberts, H.; Millar, T. J. A Survey of [D₂CO] / [H₂CO] and [N₂D⁺] / [N₂H⁺] Ratios towards Protostellar Cores. *A&A* **2007**, 471, 849–863.
- (135) Watanabe, Y.; Sakai, N.; Lindberg, J. E.; Jørgensen, J. K.; Bisschop, S. E.; Yamamoto, S. An Unbiased Spectral Line Survey toward R CrA IRS7B in the 345 GHz Window with ASTE. *ApJ* **2012**, 745, 126.
- (136) Langer, W. D.; Schloerb, F. P.; Snell, R. L.; Young, J. S. Detection of Deuterated Cyanoacetylene in the Interstellar Cloud TMC 1. *ApJ* **1980**, 239, L125–L128.
- (137) Howe, D. A.; Millar, T. J.; Schilke, P.; Walmsley, C. M. Observations of Deuterated Cyanoacetylene in Dark Clouds. *MNRAS* **1994**, 267, 59.
- (138) Cordiner, M. A.; Charnley, S. B.; Wirström, E. S.; Smith, R. G. Organic Chemistry of Low-mass Star-forming Cores. I. 7 mm Spectroscopy of Chamaeleon MMS1. *ApJ* **2012**, 744, 131.
- (139) Marcelino, N.; Cernicharo, J.; Roueff, E.; Gerin, M.; Mauersberger, R. Deuterated Thioformaldehyde in the Barnard 1 Cloud. *ApJ* **2005**, 620, 308–320.
- (140) Vastel, C.; Quénard, D.; Le Gal, R.; Wakelam, V.; Andrianasolo, A.; Caselli, P.; Vidal, T.; Ceccarelli, C.; Lefloch, B.; Bachiller, R. Sulphur Chemistry in the L1544 Pre-stellar Core. *MNRAS* **2018**, 478, 5514–5532.

- (141) Sakai, N.; Sakai, T.; Hirota, T.; Yamamoto, S. Deuterated Molecules in Warm Carbon Chain Chemistry: The L1527 Case. *ApJ* **2009**, *702*, 1025–1035.
- (142) Zucker, C.; Schlafly, E. F.; Speagle, J. S.; Green, G. M.; Portillo, S. K. N.; Finkbeiner, D. P.; Goodman, A. A. Mapping Distances across the Perseus Molecular Cloud Using CO Observations, Stellar Photometry, and Gaia DR2 Parallax Measurements. *ApJ* **2018**, *869*, 83.
- (143) Reipurth, B.; Chini, R.; Krugel, E.; Kreysa, E.; Sievers, A. Cold Dust around Herbig-Haro Energy Sources - a 1300-MICRON Survey. *A&A* **1993**, *273*, 221.
- (144) Lefloch, B.; Castets, A.; Cernicharo, J.; Langer, W. D.; Zylka, R. Cores and Cavities in NGC 1333. *A&A* **1998**, *334*, 269–279.
- (145) Lefloch, B.; Castets, A.; Cernicharo, J.; Loinard, L. Widespread SiO Emission in NGC 1333. *ApJ* **1998**, *504*, L109–L112.
- (146) Codella, C.; Bachiller, R.; Reipurth, B. Low and High Velocity SiO Emission around Young Stellar Objects. *A&A* **1999**, *343*, 585–598.
- (147) Tobin, J. J.; Looney, L. W.; Li, Z.-Y.; Chandler, C. J.; Dunham, M. M.; Segura-Cox, D.; Sadavoy, S. I.; Melis, C.; Harris, R. J.; Kratter, K.; Perez, L. The VLA Nascent Disk and Multiplicity Survey of Perseus Protostars (VANDAM). II. Multiplicity of Protostars in the Perseus Molecular Cloud. *ApJ* **2016**, *818*, 73.
- (148) Grossman, E. N.; Masson, C. R.; Sargent, A. I.; Scoville, N. Z.; Scott, S.; Woody, D. P. A Possible Protostar near HH 7-11. *ApJ* **1987**, *320*, 356–363.
- (149) Chini, R.; Reipurth, B.; Sievers, A.; Ward-Thompson, D.; Haslam, C. G. T.; Kreysa, E.; Lemke, R. Cold Dust around Herbig-Haro Energy Sources: Morphology and New Protostellar Candidates. *A&A* **1997**, *325*, 542–550.
- (150) Rodríguez, L. F.; Anglada, G.; Curiel, S. The Nature of the Radio Continuum Sources Embedded in the HH 7-11 Region and Its Surroundings. *ApJS* **1999**, *125*, 427–438.

- (151) Anglada, G.; Rodríguez, L. F.; Torrelles, J. M. Discovery of a Subarcsecond Radio Binary Associated with the SVS 13 Star in the HH 7-11 Region. *ApJ* **2000**, *542*, L123–L126.
- (152) Chen, X.; Launhardt, R.; Henning, T. IRAM-PdBI Observations of Binary Protostars. I. The Hierarchical System SVS 13 in NGC 1333. *ApJ* **2009**, *691*, 1729–1737.
- (153) Bachiller, R.; Guilloteau, S.; Gueth, F.; Tafalla, M.; Dutrey, A.; Codella, C.; Castets, A. A Molecular Jet from SVS 13B near HH 7-11. *A&A* **1998**, *339*, L49–L52.
- (154) Pickett, H. M.; Poynter, R. L.; Cohen, E. A.; Delitsky, M. L.; Pearson, J. C.; Müller, H. S. P. Submillimeter, Millimeter and Microwave Spectral Line Catalog. *J. Quant. Spectrosc. Radiat. Trans.* **1998**, *60*, 883–890.
- (155) Müller, H. S. P.; Schlöder, F.; Stutzki, J.; Winnewisser, G. The Cologne Database for Molecular Spectroscopy, CDMS: a Useful Tool for Astronomers and Spectroscopists. *Journal of Molecular Structure* **2005**, *742*, 215–227.
- (156) Ceccarelli, C.; Maret, S.; Tielens, A. G. G. M.; Castets, A.; Caux, E. Theoretical H₂CO Emission from Protostellar Envelopes. *A&A* **2003**, *410*, 587–595.
- (157) Faure, A.; Lique, F.; Wiesenfeld, L. Collisional Excitation of HC₃N by Para- and Ortho-H₂. *MNRAS* **2016**, *460*, 2103–2109.
- (158) Dubernet, M.-L. et al. BASECOL2012: A Collisional Database Repository and Web Service within the Virtual Atomic and Molecular Data Centre (VAMDC). *A&A* **2013**, *553*, A50.
- (159) Wiesenfeld, L.; Faure, A. Rotational Quenching of H₂CO by Molecular Hydrogen: Cross-sections, Rates and Pressure Broadening. *MNRAS* **2013**, *432*, 2573–2578.
- (160) Schöier, F. L.; van der Tak, F. F. S.; van Dishoeck, E. F.; Black, J. H. An Atomic and Molecular Database for Analysis of Submillimetre Line Observations. *A&A* **2005**, *432*, 369–379.

- (161) Kahane, C.; Ceccarelli, C.; Faure, A.; Caux, E. Detection of Formamide, the Simplest but Crucial Amide, in a Solar-type Protostar. *ApJ* **2013**, *763*, L38.
- (162) Wakelam, V. et al. The 2014 KIDA Network for Interstellar Chemistry. *ApJS* **2015**, *217*, 20.
- (163) Jaber Al-Edhari, A.; Ceccarelli, C.; Kahane, C.; Viti, S.; Balucani, N.; Caux, E.; Faure, A.; Lefloch, B.; Lique, F.; Mendoza, E.; Quenard, D.; Wiesenfeld, L. History of the Solar-type Protostar IRAS 16293-2422 as Told by the Cyanopolynes. *A&A* **2017**, *597*, A40.
- (164) Harrison, J. F. Relationship between the Charge Distribution and Dipole Moment Functions of CO and the Related Molecules CS, SiO, and SiS. *The Journal of Physical Chemistry A* **2006**, *110*, 10848–10857, PMID: 16970381.
- (165) Wakelam, V.; Loison, J.-C.; Mereau, R.; Ruaud, M. Binding Energies: New Values and Impact on the Efficiency of Chemical Desorption. *Molecular Astrophysics* **2017**, *6*, 22–35.
- (166) Lee, C.-F.; Li, Z.-Y.; Ho, P. T. P.; Hirano, N.; Zhang, Q.; Shang, H. Formation and Atmosphere of Complex Organic Molecules of the HH 212 Protostellar Disk. *ApJ* **2017**, *843*, 27.
- (167) Codella, C. et al. Water and interstellar complex organics associated with the HH 212 protostellar disc. On disc atmospheres, disc winds, and accretion shocks. *A&A* **2018**, *617*, A10.
- (168) Lee, C.-F.; Kwon, W.; Jhan, K.-S.; Hirano, N.; Hwang, H.-C.; Lai, S.-P.; Ching, T.-C.; Rao, R.; Ho, P. T. P. A Pseudodisk Threaded with a Toroidal and Pinched Poloidal Magnetic Field Morphology in the HH 211 Protostellar System. *ApJ* **2019**, *879*, 101.
- (169) Lee, C.-F.; Li, Z.-Y.; Ho, P. T. P.; Hirano, N.; Zhang, Q.; Shang, H. First detection of equatorial dark dust lane in a protostellar disk at submillimeter wavelength. *Science Advances* **2017**, *3*, e1602935.
- (170) Codella, C.; Podio, L.; Fontani, F.; Jimenez-Serra, I.; Caselli, P.; Palumbo, M. E.; López-Sepulcre, A.; Beltrán, M. T.; Lefloch, B.; Brucato, J. R.; Viti, S.; Testi, L. Complex organic

molecules in protostellar environments in the SKA era. *Advancing Astrophysics with the Square Kilometre Array (AASKA14)*. 2015; p 123.